Challenge Journal of
# STRUCTURAL MECHANICS

Vol.5 No.4 (2019)

Mindlin's theory buckling building codes
dynamic analysis dynamic response
earthquake elastic foundation finite
element analysis finite element
method nonlinear analysis operational
modal analysis optimization prestressing
pushover analysis reinforced concrete
seismic analysis seismic design
seismic isolation soil-structure interaction
temperature effects thick plate wind

TULPAR
ACADEMIC PUBLISHING

ISSN 2149-8024

Challenge Journal of Structural Mechanics

**E-mail:** *cjsmec@challengejournal.com*

**Web page:** *cjsmec.challengejournal.com*

**TULPAR Academic Publishing**
*www.tulparpublishing.com*

Challenge Journal of Structural Mechanics

# CONTENTS

## *Research Articles*



TULPAR ACADEMIC PUBLISHING

Challenge Journal of Structural Mechanics

Research Article

# Analysis of historical structures by using finite element method in Iznik Yeşil Mosque

Aykut Uray [a,*], H. Selim Şengel [a], Serdar Çarbaş [b]

[a] *Department of Civil Engineering, Eskişehir Osmangazi University, 26480 Eskişehir, Turkey*
[b] *Department of Civil Engineering, Karamanoğlu Mehmetbey University, 70100 Karaman, Turkey*

**ABSTRACT**

In this study, non-destructive tests and laboratory tests were carried out in order to determine the material properties in Iznik Yeşil Mosque, Iznik District, Bursa Province. For the purpose of determining the soil characteristics of the building, the soil survey studies conducted in the Iznik Yeşil Mosque area were investigated. The finite element model was formed by making a three dimensional model study of the structure. With the finite element model, static analysis, modal analysis and behavioral spectrum analysis were performed under vertical loads in order to collect data for the damaged areas of the structure.

**ARTICLE INFO**

*Article history:*
Received 25 March 2019
Revised 16 May 2019
Accepted 15 June 2019

*Keywords:*
Static analysis
Historical structures
Ultrasound test
Finite element method

## 1. Introduction

Over the centuries, historical buildings have suffered from earthquakes, fires, wars, negative environmental conditions, along with the formation of periodic indifference. A part of these important and valuable structures have been lost, while another part have faced structural losses and some have survived to the present day. Today, many scientists continue their work on preservation of historical heritage. The preservation of Historical structures is very important in terms of development and sustainability of the understanding of interdisciplinary studies. The role of civil engineering in Interdisciplinary study is to examine the element and material properties of historical masonry structures, to investigate retrofitting techniques that can be applied to historical masonry structures, to create a building model and to make static and dynamic analysis on the model. Material analysis of the structure of Iznik Yeşil Mosque was carried out and the necessary parameters were determined in order to make the related calculations. Static and dynamic analysis were made according to these parameters.

In the modeling and analysis of Historical structures, studies are done by using the finite element model. For this purpose, the finite element method is compared with the manual calculations, in order to do so a sample model was created and the results of calculations were compared.

## 2. Analysis with Finite Element Method

### *2.1. Comparison of sample models and analysis*

The analysis of Finite element method can be performed manually or by computer, and can be compared as shown in Fig. 1, a sample arch model was created and studies were made. The displacement value on the ninth node point was controlled in two directions by performing a loading of 1 kN at the center of the belt. The Sap2000 program was used for the computerized studies (Sap2000 Manual, 2005). In the manual calculation method, as shown in Fig. 2, operations were performed using the local stiffness matrix of the plane frame element (Uray, 2018).

It was found that there were 0.039 m displacement values at the ninth node with the two methods. In manual analysis studies, the selection of the stiffness matrix

* *Corresponding author*. Tel.: +90-222-712-5305 ; E-mail address: aykuturay@gmail.com (A. Uray)
ISSN: 2149-8024 / DOI: https://doi.org/10.20528/cjsmec.2019.04.001

of the element is very important. While it is possible to perform a finite element analysis on a single element, it is very difficult to manually calculate complex structures with more than one element. Therefore, modeling and analyzing historical structures in a computer environment will give closer results to reality.

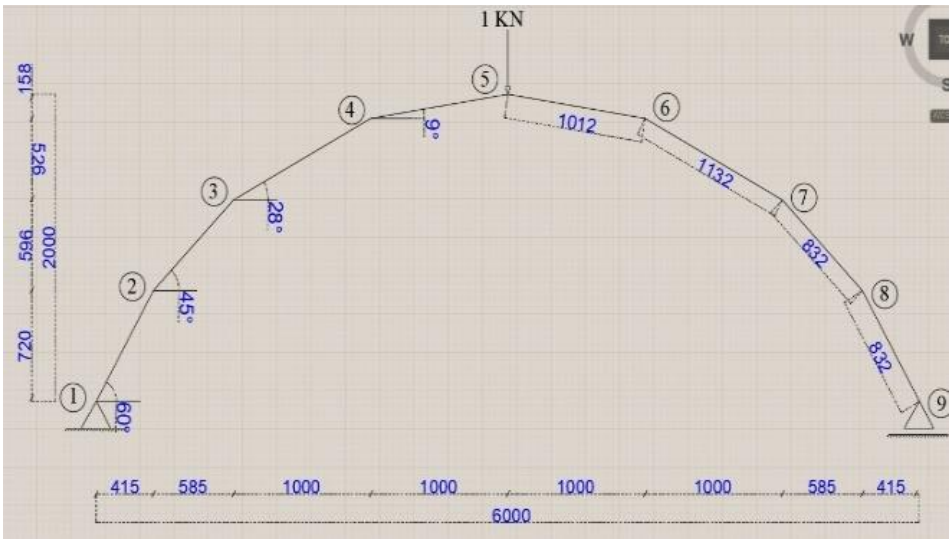


**Fig. 1.** Sample arch model.

$$\hat{\underline{k}} = \begin{bmatrix} \frac{EA}{L} & 0 & 0 & -\frac{EA}{L} & 0 & 0 \\ 0 & \frac{12EI_3}{L^3} & \frac{6EI_3}{L^2} & 0 & -\frac{12EI_3}{L^3} & \frac{6EI_3}{L^2} \\ 0 & \frac{6EI_3}{L^2} & \frac{4EI_3}{L} & 0 & -\frac{6EI_3}{L^2} & \frac{2EI_3}{L} \\ -\frac{EA}{L} & 0 & 0 & \frac{EA}{L} & 0 & 0 \\ 0 & -\frac{12EI_3}{L^3} & -\frac{6EI_3}{L^2} & 0 & \frac{12EI_3}{L^3} & -\frac{6EI_3}{L^2} \\ 0 & \frac{6EI_3}{L^2} & \frac{2EI_3}{L} & 0 & -\frac{6EI_3}{L^2} & \frac{4EI_3}{L} \end{bmatrix}$$

**Fig. 2.** Stiffness matrix of plane frame element.

## 3. Iznik Yeşil Mosque as an Example and Previous Studies

The construction of the mosque in Iznik District of Bursa Province was commenced in 1378 according to the inscriptions. When the construction of the mosque was completed, it was opened for worship and since that date it has become one of the important centers of Iznik region. By making static and dynamic analyses of this important work, the situation after a possible earthquake was examined and a roadmap was created to take the necessary security precautions.

Iznik Yeşil Mosque, with its rectangular plan extending in the north-south direction, the main place of worship is covered with a single dome and the last congregation is located on the northern facade, the structure is a single domed mosque. The reason why the building is called the Green Mosque is that it is mainly covered with turquoise tiles and glazed bricks covering the entire area from the base of the minaret to the lead cone. The structure has overall dimensions of 26.20x14.25 meters. The last main body walls thicknesses are between 1.70 m and 1.80 m and are made entirely of marble. The single-domed structure consists of a space with an overall size of 13.50 meters. It has a minaret built as an integrated structure. While the last congregational walls outer elevation reaches 9.55 meters, the outer body walls elevations of the main meeting section reach 8.50 m. The upper elevation of the main dome appears to be 18.30 meters.

The mosque in general, in the present process, is well preserved and without losing its general architectural features. The original state was generally preserved. Since the areas around the mosque were far from being built, serious deformations were not observed due to ground movements on the main body walls of the mosque. In the mosque, which has a rectangular plan with its north-south direction, two granite column elements are found when the last congregation is taken from the neighborhood to the three-eyed entrance area (Fig. 3.).

**Fig. 3.** Entrance to the west facade of the mosque - deformation formed column and area.

### *3.1. Determination of the modulus of elasticity with onsite and laboratory tests*

In order to provide accurate results of the static and dynamic analyses to be made after the modelling of the mosque, studies have been done with the ultrasound test method within the mosque. Tests were conducted in the laboratory environment for determining unit volume weights by using materials belonging to the structure body walls, which were previously separated from the building but collected during restoration work. The results were performed by ultrasound testing in seven different regions of the mosque. The columns in the last communion section, the columns in the entrance part of the mosque and the body walls were conducted. In the Yeşil Mosque during the restoration work between the years 2015-2016, the location of the main body wall and column elements-which could not be detected- in the mosque under the storage of the granite elements in the laboratory environment. The average value was calculated by performing unit volume weight tests (Table 1).

The values obtained as a result of tests performed in Situ and laboratory environment were determined by using Eqs. (1) and (2) from empirical formulas found in the literature and modulus of elasticity of the elements (Bağbancı, 2009; Anonymous, 2018). With Eqs. (1) and (2), after the determination of the unit weight values in laboratory environment with the determined sound transition time ($\mu s$) at certain length intervals as a result of the ultrasound tests performed on site, the average elasticity module determination of the tested area of the structure was made with the help of the empirical formulas in the literature.

$$E = \left(\frac{L}{t}\right)^2 \gamma \, 10^3 \tag{1}$$

$$E = Cl^2 \, Q \;\; (1+\gamma) \;\; (1-2\gamma) \;/\; (1-\gamma) \tag{2}$$

In samples, the sound transition time, volume weights of the materials and empirical formulas were utilized, as shown in Table 1, the determination of static modulus of elasticity of the elements was performed. The values found were high and close to the values given in the literature of granite stones which are the main material of the mosque. Although the same values in all parts of the structure are generally the same, the mosque entrance facade of the damaged position on the west side of the carrier column element is determined that the values are low compared to other elements.

### *3.2. Finite element model of the structure*

Key Creator (2004) software program was used to design a three-dimensional structure for the creation of the finite element model of the structure. In the restoration and restitution projects with the survey drawings, the

planning, section, appearance and detail sheets were used to carry out the dimensioning process. Primarily, the columns of the building and the body walls were modeled. After modeling of the body walls in General, gaps were created on the structure, such as the windows and doors. In the last part, the structure was designed as a three-dimensional design of the building elements used as the dome, vault, etc. (Fig. 4).

**Table 1.** Determination of modulus of elasticity.

| | | | | | Formula-1 | Formula-2 | | |
|---|---|---|---|---|---|---|---|---|
| Sample Place | Number of Tests | Length (L) (mm) | Sound Transition Time (μs) | Unit Volume Weight ($gr/cm^3$) | Static Modulus of Elasticity ($N/mm^2$) | Static Modulus of Elasticity ($N/mm^2$) | Average Static Modulus of Elasticity ($N/mm^2$) | Static Modulus of Elasticity ($kN/m^2$) |
| Mosque Entrance East Facade Column - 1 | 1 | 340.00 | 62.80 | 2.67 | 78,261.80 | 72,077.20 | 51,300.19 | $51*10^6$ |
| | 2 | 200.00 | 39.10 | 2.67 | 69,858.26 | 64,337.75 | | |
| | 3 | 800.00 | 209.30 | 2.67 | 39,007.92 | 35,925.34 | | |
| | 4 | 780.00 | 206.10 | 2.67 | 38,242.34 | 35,220.26 | | |
| | 5 | 800.00 | 177.00 | 2.67 | 54,543.71 | 50,233.43 | | |
| | 6 | 800.00 | 177.40 | 2.67 | 54,298.02 | 50,007.15 | | |
| Mosque Entrance West Facade Column - 2 | 1 | 340.00 | 75.50 | 2.67 | 54,147.10 | 49,868.16 | 26,751.20 | $26*10^6$ |
| | 2 | 200.00 | 63.30 | 2.67 | 26,654.09 | 24,547.77 | | |
| | 3 | 740.00 | 302.60 | 2.67 | 15,967.50 | 14,705.68 | | |
| | 4 | 730.00 | 365.00 | 2.67 | 10,680.00 | 9,836.02 | | |
| | 5 | 740.00 | 174.40 | 2.67 | 48,070.84 | 44,272.07 | | |
| | 6 | 740.00 | 215.00 | 2.67 | 31,629.90 | 29,130.36 | | |
| | 7 | 750.00 | 304.70 | 2.67 | 16,176.66 | 14,898.31 | | |
| The Main Body Wall of the Last Communion Facade | 1 | 200.00 | 32.60 | 2.67 | 100,493.06 | 92,551.65 | 51,472.19 | $51*10^6$ |
| | 2 | 200.00 | 51.50 | 2.67 | 40,267.70 | 37,085.57 | | |
| | 3 | 200.00 | 56.00 | 2.67 | 34,056.12 | 31,364.86 | | |
| | 4 | 200.00 | 59.40 | 2.67 | 30,269.02 | 27,877.03 | | |
| | 5 | 200.00 | 53.50 | 2.67 | 37,313.30 | 34,364.64 | | |
| | 6 | 200.00 | 33.90 | 2.67 | 92,933.41 | 85,589.40 | | |
| Mosque Last Communion East Column -1 | 1 | 200.00 | 32.70 | 2.67 | 99,879.36 | 91,986.45 | 100,986.24 | $100*10^6$ |
| | 2 | 300.00 | 42.60 | 2.67 | 132,414.2 | 121,950.25 | | |
| | 3 | 500.00 | 83.10 | 2.67 | 96,660.54 | 89,022.00 | | |
| Mosque Last Communion Column -2 | 1 | 200.00 | 38.10 | 2.67 | 73,573.48 | 67,759.38 | 75,425.32 | $75*10^6$ |
| | 2 | 330.00 | 57.10 | 2.67 | 89,179.89 | 82,132.50 | | |
| | 3 | 520.00 | 93.30 | 2.67 | 82,938.21 | 76,384.07 | | |
| Mosque Last Communion Column -3 | 1 | 200.00 | 31.50 | 2.67 | 107,634.1 | 99,128.44 | 96,221.51 | $96*10^6$ |
| | 2 | 310.00 | 48.20 | 2.67 | 110,443.6 | 101,715.87 | | |
| | 3 | 600.00 | 100.40 | 2.67 | 95,355.63 | 87,820.21 | | |
| Mosque East Front Main Body Wall | 1 | 200.00 | 34.30 | 2.67 | 90,778.50 | 83,604.79 | 65,348.64 | $65*10^6$ |
| | 2 | 200.00 | 40.20 | 2.67 | 66,087.47 | 60,864.95 | | |
| | 3 | 200.00 | 38.60 | 2.67 | 71,679.78 | 66,015.33 | | |
| | 4 | 200.00 | 31.90 | 2.67 | 104,951.8 | 96,658.05 | | |
| | 5 | 200.00 | 52.00 | 2.67 | 39,497.04 | 36,375.81 | | |
| | 6 | 200.00 | 45.00 | 2.67 | 52,740.74 | 48,572.94 | | |

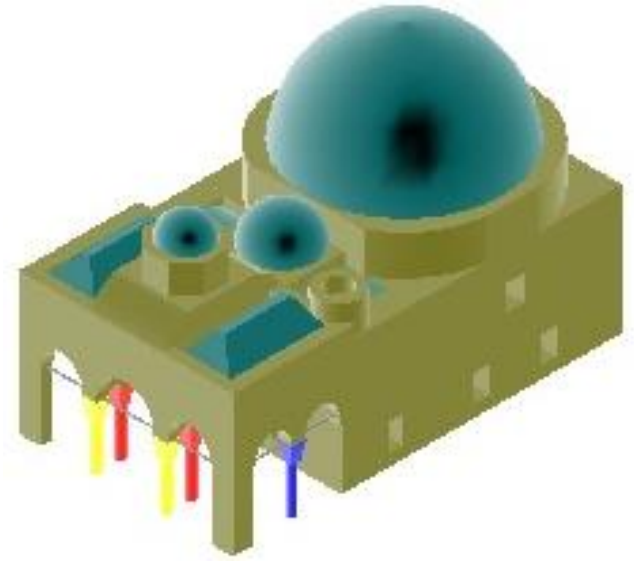

**Fig. 4.** Three-dimensional modelling of the structure.

The construction of the finite element model and the analysis of the structure to be done in detail, the columns of the entrance part of the mosque, the last communion columns, the main body walls, the wooden tensioner dome, the vaulted building elements are modeled separately.

The elements found in the model were divided into eight main parts and the descriptions were made. All elements in the structure are designed as solid elements. With the creation of finite elements, the structure consisted of 117709 solid elements, 38018 solid element net surface and 101420 node points (Fig. 5). Considering that the finite element networks are changed accurately in proportion to the accuracy of the analysis results, the reduction of finite element network sizes will ensure more accurate results in analysis. Analysis studies were conducted using ALGOR finite element software (2007) for modeling and analysis of the finite element model.

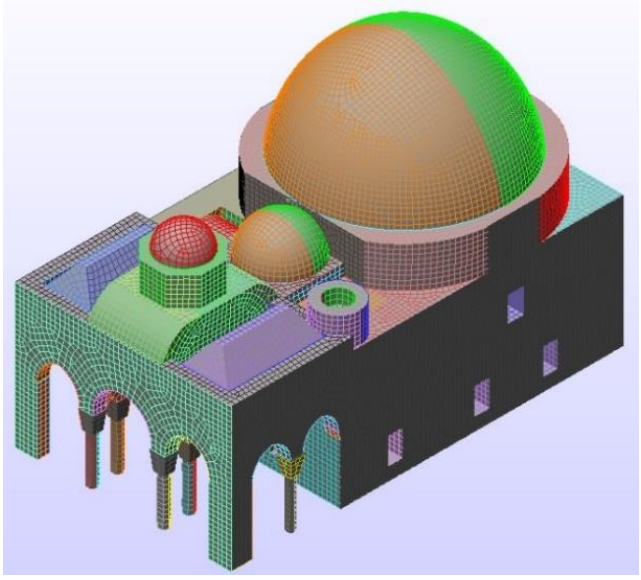

**Fig. 5.** Finite element model of the structure.

### *3.3. Analysis of the structure*

A static analysis of the Structure under vertical loads is very important to see the stress clutter and distribution that may occur under the vertical loads of the structure, the cracks that may occur in the structure and the non-plane movements and displacements. It provides an understanding of the behaviour of the building on which it has to carry continuously. In the analysis, excluding other loads that may affect the structure, it is important to see how the vertical loads are likely to create deformation in the structure and to take precautions with an appropriate technique. When the current situation of the Yeşil Mosque is examined, a number of deformations are thought to occur in the minaret in the north-west section with the effect of vertical loads. Studies have been conducted to investigate these parts in the analyses to be done.

#### *3.3.1. Static analysis under vertical loads*

Two analysis studies were carried out under vertical loads for this structure. In the first analysis, the material properties are considered to be the same according to the material genus, and in the analysis under the second-to-be-vertical loads, the data that is obtained as a result of non-destructive testing of damaged zone values were analyzed by injury. The goal here is to compare the situation we think is not damaged by today's situation. In Tables 2 and 3, the values were taken according to the characteristics of the element.

**Table 2.** Analysis parameters under vertical loads (First Analysis).

| | Stone | Brick |
|---|---|---|
| Pressure Strength (MPa) | 50 MPa | 20 MPa |
| Tensile Strength in Bending (MPa) | 5 MPa | 3.9 MPa |
| Modulus of Elasticity ($N/m^2$) | $50*10^9$ $N/m^2$ | $5*10^9$ $N/m^2$ |
| Unit Volume Weight ($kg/m^3$) | 2607 $kg/m^3$ | 1600 $kg/m^3$ |
| Slip Module ($N/m^2$) | $21*10^9$ $N/m^2$ | $2.1*10^9$ $N/m^2$ |

**Table 3.** Analysis parameters under vertical loads (Second Analysis).

| | Stone - 1 | Stone - 2 | Brick |
|---|---|---|---|
| Pressure Strength (MPa) | 50 MPa | 50 MPa | 20 MPa |
| Tensile Strength in Bending (MPa) | 5 MPa | 5 MPa | 3.9 MPa |
| Modulus of Elasticity ($N/m^2$) | $50*10^9$ $N/m^2$ | $26*10^9$ $N/m^2$ | $5*10^9$ $N/m^2$ |
| Unit Volume Weight ($kg/m^3$) | 2607 $kg/m^3$ | 2607 $kg/m^3$ | 1600 $kg/m^3$ |
| Slip Module ($N/m^2$) | $21*10^9$ $N/m^2$ | $11*10^9$ $N/m^2$ | $2.1*10^9$ $N/m^2$ |

After determining the parameters in relation to the analysis of the structure and under its self-weight power, we find that it was carried out with the effect of 9.81456 m/sn$^2$ gravitational acceleration in Z direction. In the structure, the minaret built into the mosque is made up of three-dimensional modeling of a certain quota, the vertical loads formed due to the non-model part are done by mathematical calculations – in the cylinder section in Z direction-the program is defined as a load of 1,500 KN. In accordance with the specified parameters, the values are transferred to the structure and the finite element node points sitting on the floor are determined to do not take the moment in the three directions.

In two analyses of the structure under vertical loads, the structure was observed to be good under vertical loads, in which the structure worked in the pressure. While the two analyses have been observed to be closely related to the vertical displacement values in general, the second analysis is done with the values determined by experimental methods of the column that we described as damaged nowadays, the whole structure was affected by the column elements, especially the stresses, the residuals were observed in the columns. When we look at the sections with stresses, from the current state of the structure, the mosque coincided with partial deformations in the last Communion entrance section, and the tension of the glass in the column by the west of the entrance part of the window was formed, the damage can be started in this region (Figs. 6-9).

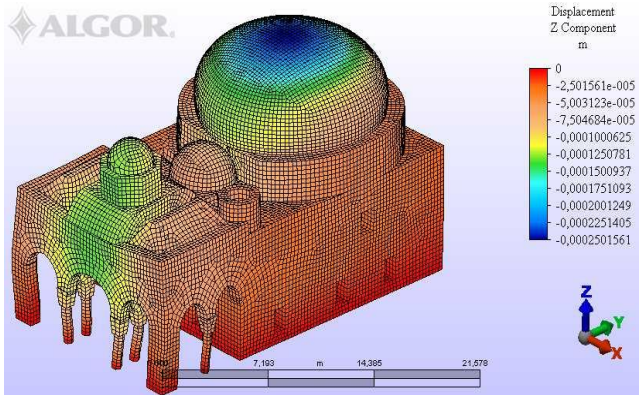


**Fig. 6.** Static analysis made under vertical loads – vertical direction displacement (First Analysis).

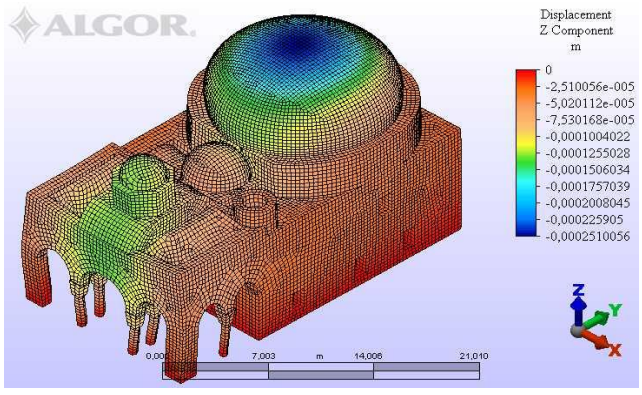


**Fig. 7.** Static analysis made under vertical loads – vertical direction displacement (Second Analysis).

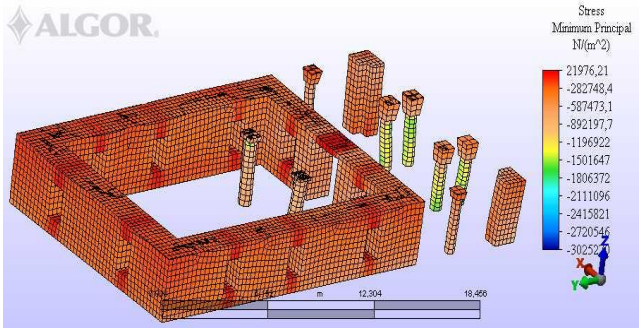


**Fig. 8.** Static analysis made under vertical loads – stresses occurring in columns (First Analysis).

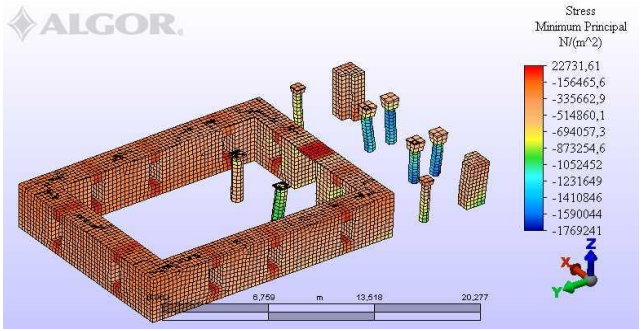


**Fig. 9.** Static analysis made under vertical loads – stresses occurring in columns (Second Analysis).

### *3.3.2. Earthquake analysis*

Different from the static analysis of earthquake analyses to examine the behavior of the structure under loads that change over time, the inertia forces formed by the structure due to earthquake forces. Inertial forces are the forces that resist the acceleration of the construction movement with the effect of horizontal loads from the outside. Natural vibration periods are very important for determining the calculations of structures by performing earthquake analysis. Self-worth analysis or modal analysis are the methods used to see the mode shapes of structures and the periods of free vibration. The finite element model of ızınik Yeşil mosque has been performed with the aid of the ALGOR program and has been undergoing modal analysis and has been checked for 10 modes. The mode of vibration, which belongs to a free vibration period, is expressed by the mass participation rate, in which the total mass of the structure can be triggered and incorporated into the oscillation movement (Dabanlı, 2008). Table 4 shows the free vibration periods, modal frequencies, and mass participation ratios of the structure's 10 calculated modes. As a result of the analyses, the entire structure is lateral movement In X-Direction (East-West). The First mode's vibration frequency value is 20.547 Hz and the mass participation rate is 60.99%. In the third mode of the Structure, lateral movement in the Y direction (North-South). The vibration frequency value of the Third mode is 24.87 Hz and the mass participation rate is 41.05%.In the analysis made through 10 Modes, the total turnout rate in the X direction was 74.90%, while the total participation rate in the Y direction was 69.48% and 7.7% in the Z direction.

**Table 4.** Free vibration cycles of the structure, modal frequency and mass participation rates.

| Mode | Frequency (Hz) | Period (sn) | Mass participation X (%) | Mass participation Y (%) | Mass participation Z (%) |
|---|---|---|---|---|---|
| 1 | 20.547 | 0.04866891 | 60.99 | 0 | 0 |
| 2 | 24.162 | 0.0413873 | 1.9 | 0,65 | 0 |
| 3 | 24.870 | 0.04020909 | 0.02 | 41,05 | 0,05 |
| 4 | 29.022 | 0.03445662 | 0.01 | 10,94 | 0 |
| 5 | 31.690 | 0.0315557 | 3.36 | 0,09 | 0 |
| 6 | 34.069 | 0.0293522 | 0.01 | 15,7 | 0 |
| 7 | 38.750 | 0.02580645 | 8.53 | 0,01 | 0,02 |
| 8 | 39.115 | 0.02556564 | 0.05 | 0 | 4,95 |
| 9 | 44.880 | 0.02228164 | 0.03 | 0 | 0,01 |
| 10 | 45.500 | 0.02197802 | 0 | 1,04 | 2,56 |
| Total Participation Rates: | | | 74.90 | 69.48 | 7.7 |

The torsional movement was observed in the mode where the Structure was active in the X and Y direction. The first mode is the dominant mode in the X direction (Fig. 10a), the third mode (Fig. 10b) is the dominant mode in the Y direction.

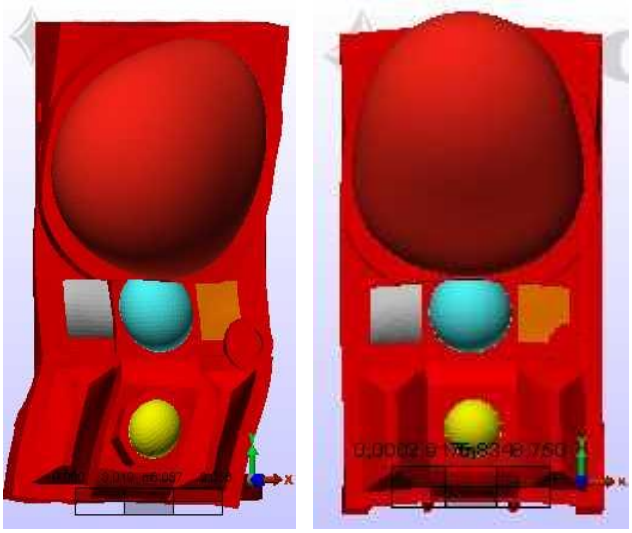

(a) (b)

**Fig. 10.** The dominant modes in the X and Y direction.

In Earthquake analyses, calculations and analyses were made by utilizing spectrum analyses in the 2.4 section of "Regulation On Buildings To be held in Earthquake Zones". The Spectrum calculations were made using the "Full-Frame Consolidation" method. The values used in the Analyses are used in the formulas contained in the relevant substances of the regulation to create the acceleration spectrum chart (DBYYHY, 2007). The acceleration sprectrum chart was created using formulas (Fig. 11).

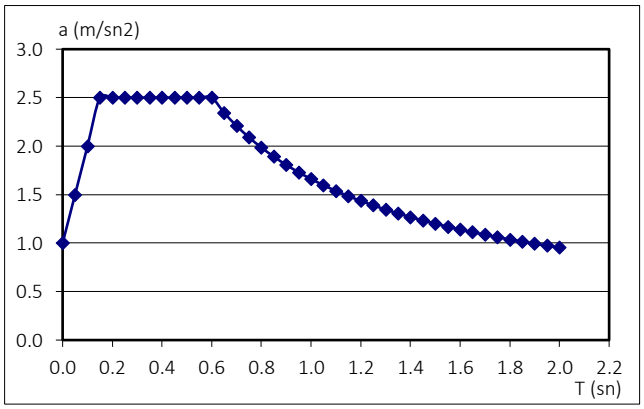


**Fig. 11.** Acceleration spectrum graph.

Earthquake analyses were made in the X and Y direction of the structure. As a result of earthquake analyses in the X direction, 0.10 mm displacement occurred as shown in Fig. 12 in the first mode of the dome cover with the largest mass participation, In the last congregation part of the structure, the columns and wall building elements in the upper cover section, It was found that there was a displacement of 0.60 mm. In other regions of the structure, the displacement values in the X direction are generally low.

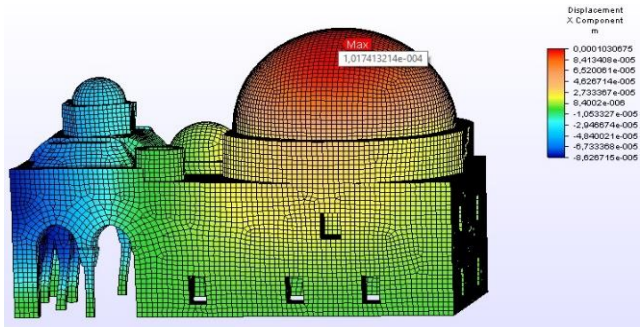


**Fig. 12.** X-direction displacement value in dome resulting from earthquake analysis in X direction.

When the stresses of the analysis were examined, it was observed that the maximum stresses were between 10.56 MPa and 19.90 MPa (Fig. 13). According to the modalities of the building, when the values they have taken are examined, it was determined that the main dome pulley and the Turkish triangles were formed in the corners of the main body walls and these values were in the range of 0.8-1.0 MPa. And here we can be say that the structure generally does not consist of serious deformations in the X direction, it shows a good structural behavior.

As a result of earthquake analysis in the Y direction, the maximum displacement in the third mode of mass participation occurred in the dome cover of the structure and it was identified with the value 0.62 mm. (Fig. 14). In the fourth and sixth mode of the structure, the displacement of the Y direction between 0.11 and 0.13 mm was determined in the last communion section of the regions where the displacement occurred and the upper cover elements of the mosque entrance area.

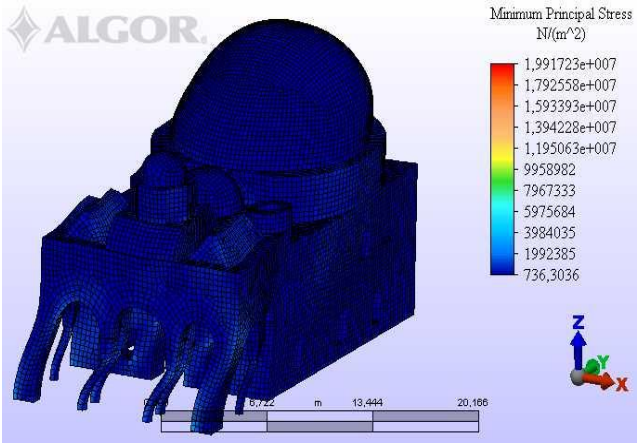


**Fig. 13.** Maximum stresses in x direction resulting from earthquake analysis in X.

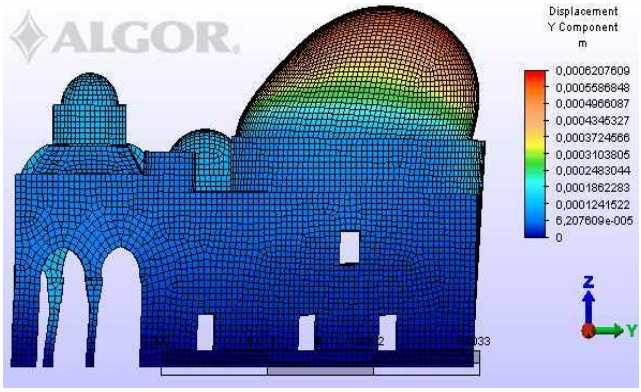


**Fig. 14.** Displacement values of the dome in the Y direction as a result of earthquake analysis.

## 4. Conclusions

In this study, the structure was aimed to determine the behavior of the earthquake with the behavior of the structure under vertical loads by performing static and dynamic analyses with finite element method. In addition, based on the current state of the structure, the deformation of the structure is aimed to determine the analyses. Dynamic Analysis studies for 2007, regulation on structures to be made in Earthquake regions is used. In order to determine the material parameters, ultrasound tests and unit volume weight tests were performed in laboratory, and the analysis parameters were determined. By creating the three-dimensional model of the structure, the data were analyzed by static analysis, modal analysis and behavioral spectrum analysis, stress values, displacement values and performance of the structure.

When the current situation of the Structure is examined, the entrance part of the mosque was observed to have deformations in the column and header on the Western Front. As a result of the static analyses of the structure under vertical loads, the stress stacks were observed to occur in the header of the damaged column and it has been determined that the model, experiments and analyses overlap with the current state of the mosque.

As a result of static analysis of the structure under vertical loads, the maximum displacement is on the main dome cover and the values were around 0.25 mm, but when we examined structure, there were no visible deformation in the main dome. However, if the structure was repaired in the Sixties and intervention was carried out, the repair production is thought to be performed during this period.

In the structure, two vertical loads were performed under static analysis, and the results of the two analyses were similar, compared to each other. As a result of the static analysis of the structure under the vertical loads, the values were observed in the columns made of mono blocks, and when the tension readings were examined, there was more pressure stresses throughout the structure. However, the analysis study carried out values according to the parameters calculated in the damaged column together with the tests performed in place, the property was observed that the loads and displacement values from all the columns were increased, the last communion was found in the corner walls.

When the modal analysis and behavioral spectrum analyses were examined in the Structure, the first mode in the X direction was the prevailing mode, and in the Y direction, the prevailing mode was the third mode. When the mode shapes of the Structure are examined, the movement can be traced in the east-west and north-south direction. It was found that the earthquake loads caused a maximum displacement of 0.60 mm in the structure, and the study have revealed that the displacement value could be at most in the last congregation top cover. In the earthquake analysis carried out X (east-west) in the direction of the pressure stress values of the structure, it was determined that the final congregation was formed in the top cover and walls and the tensile values were around 10 MPa. Similarly, the results of the earthquake analysis in the direction of the Y and the values of the last communion in the upper cover section of 6 MPa can consist of regressive. In the case of an earthquake, the formation of deformations and cracks in the last communion section is likely to occur when the structure have been seen by modal analysis and behavioral spectrum analyses.

Considering the strengthening situation of the building today, the damaged column and the stainless-steel lathes made in the head are considered to be sufficient for the current state of the structure. It is considered that there is no serious construction in the area around Iznik Yeşil Mosque and therefore the problems that may arise from the ground do not appear in the structure. For this to be sustainable, it is advisable to make the construction around the mosque so that it does not allow the production to be made to disrupt the ground balance.

With the impact of the earthquake forces to influence the structure, it is not possible to take precautions for the deformations that may occur in the last congregation part of the structure as a weak zone. However, it is important for the overall structure of the building to take necessary measures together with a deformation that may occur by monitoring the movements of the building.

## Acknowledgements

The authors solemnly acknowledge the various researchers who have published their experimental results that were used in this study.

## References

ALGOR V20.00 (2007). Autodesk Inc., U.S.A.

Anonymous (2018). University of Colorado, Integrated Teaching & Learning Laboratory Ultrasound Test, https://itll.colorado.edu/

Bağbancı MB (2009). Analysis of Historical Structures by Finite Element Method in the Case of Bursa Ördekli Bath. *Ph.D thesis*, Uludağ University, Bursa.

Dabanlı Ö (2008). Determination of Earthquake Performance of Historical Masonry Structures. *M.Sc. thesis*, İstanbul Technical University, Istanbul.

DBYYHY (2007). Regulation on Structures in Earthquake Regions, March, 2007.

KEY CREATOR V4.0.0 (2004). Cubotek Corporation, U.S.A.

Sap2000 Manual (2005). Integrated Structural Analysis and Design Software, Computer and Structures Inc., Berkeley, California.

Uray A (2018). Determination of Earthquake Performance of Historical Masonry Structures. *M.Sc thesis*, Eskisehir Osmangazi University, Institute of Science and Technology, Eskisehir.

Challenge Journal of Structural Mechanics

Research Article

# Optimization of PID controller parameters for active control of single degree of freedom structures

Serdar Ulusoy [a,*], Sinan Melih Niğdeli [b], Gebrail Bekdaş [b]

[a] *Department of Civil Engineering, Yeditepe University, 34755 İstanbul, Turkey*
[b] *Department of Civil Engineering, İstanbul University-Cerrahpaşa, 34320 İstanbul, Turkey*

**ABSTRACT**

In active control of structures, the parameters of controllers used application must be perfectly tuned. In that case, a good vibration reduction performance can be obtained without a stability problem. During the tuning process, the limit of control force and time delay of controller system must be considered for applicable design. In the study, the optimum parameters of Proportional-Derivative-Integral (PID) type controllers that are proportional gain ($K$), integral time ($T_i$) and derivative time ($T_d$) were optimized by using teaching learning-based optimization (TLBO). TLBO is a metaheuristic algorithm imitating the teaching and learning phases of education in classroom. The optimization was done according to the responses of the structure under a directivity pulse of near fault ground motions. In the study, time delay was considered as 20 ms and the optimum parameters of PID controller for a single degree of freedom (SDOF) structural model was found for different control force limits. The performances and feasibility of the method were evaluated by using sets of near fault earthquake records.

**ARTICLE INFO**

*Article history:*
Received 6 September 2019
Revised 29 October 2019
Accepted 4 November 2019

*Keywords:*
Active control
PID controller
Teaching-learning based optimization
Control force

## 1. Introduction

In structural control, active control methods are generally the best option due to high energy damping, but practical application of active control systems is not preferred because of several disadvantages. These disadvantages are time delay, stability problem and physical application of control force. These factors need to be detailly investigated.

In the last decade, several studies about active control of structures have been conducted. These studies include several types of control algorithms such as proportional integral (PID) (Nigdeli and Boduroğlu, 2013; Ulusoy et al, 2018; Nigdeli and Boduroğlu, 2014) H∞ control (Chang and Lin, 2009; Lin et al., 2010) direct adaptive control (Bitaraf et al., 2012), wavelet-based adaptive pole assignment control (Amini and Samani, 2014), self-constructing wavelet neural network algorithm (Wang and Adeli, 2015), decentralized network control (Bakule et al., 2016), sliding mode control (Yang et al., 1997; Wu et al., 1998), linear quadratic regulator (LQR) (Aldemir and Bakioğlu, 2001) and fuzzy control (Nazarimofrad and Zahrai, 2017) to reduce the structural responses and to investigate some disadvantages of control systems.

In the present study, active tendon control of structure was presented by using PID type controllers. The tuning of PID controller was done by employing a metaheuristic method called teaching learning-based optimization (TLBO) (Rao et al., 2011). The performance of the system is evaluated by using different control force limits and a wide range historical ground motions presented in FEMA P695: Quantification of Building Seismic Performance Factors (FEMA, 2009).

## 2. Methodology

In Fig. 1, a single degree of freedom (SDOF) structure with active tendons is shown. The structural parameters

* *Corresponding author*. E-mail address: serulusoy87@gmail.com (S. Ulusoy)
ISSN: 2149-8024 / DOI: https://doi.org/10.20528/cjsmec.2019.04.002

such as mass, stiffness and damping coefficients are shown as $m_1$, $k_1$ and $c_1$, respectively. $R$ is the pre-stress force, which is adjusted at control of structure in dynamic state. The properties of tendon are the stiffness ($k_c$) and angle respect to ground ($\alpha$). $u_1$ is the control signal provided by PID controller. The equation of motion and the equation of control signal ($u_1$) are given as Eqs. (1) and (2), respectively. The PID parameters are proportional gain ($K_p$), Integral Time ($T_i$) and derivative time ($T_d$) and these parameters are optimized. $e(t)$ is the error signal, which is taken as the velocity of structure respect to ground ($\dot{x}_1$). $x_1$ is the displacement of structure and the earthquake acceleration is shown as $\ddot{x}_\sigma$.

$$m_1\ddot{x}(1)+c_1\dot{x}(t)+k_1x(t)=-m_1\ddot{x}_g-4k_cu_1\cos\alpha \quad (1)$$

$$u_1=K_P\left[e(t)+\frac{1}{T_i}\int_0^t e(t)dt+T_d\frac{de(t)}{dt}\right] \quad (2)$$

$$e(t)=x_r-x \quad (3)$$

$x_r$ is taken as zero to minimize the displacement of structure. In that case, the final equation of control signal is as follows:

$$u_1=K_P\left[-x+\frac{1}{T_i}\int_0^t -xdt+T_d\frac{d}{dt}\right] \quad (4)$$

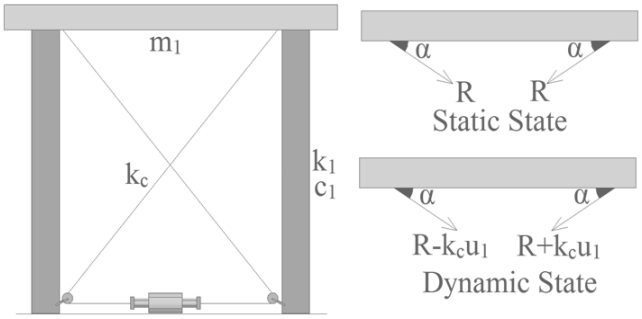


**Fig. 1.** The shear building model.

During the optimization process, a directivity pulse with 1.5s period and 230 cm/s peak ground velocity is used. The near fault pulse is generated according to the equations of Makris (Makris, 1997). The delay of control signal is taken as 20ms. A limit taken for the control signal and the objective function is penalized for the violations of the limit. The stages of the optimization process are summarized as follows:

- Define problem parameters and ranges of design variables (PID controller parameters)
- Generate candidate design variable solutions randomly and calculate the objective function value by using dynamic analysis.
- Start optimization process.
- Modify existing candidate solutions by using teacher phase considering the best existing solution and update solutions with minimum objective function.
- Modify existing candidate solutions by using learner phase considering two existing solutions and update solutions with minimum objective function.
- Continue optimization process for several iterations.

## 3. Numerical Examples

The constant parameters such as $m_1$, $k_1$, $c_1$, $\alpha$ and $k_c$ are 2924 kg, 1.39 MN/m, 1.581 kNs/m, 360 and 372.1 kN/m, respectively. The maximum control force is limited to 10%, 30% and 50% of the weight of the structure. The optimum results are given as Table 1 and flowchart of the optimization process is given in Fig. 2. The maximum displacement under impulsive pulse is 3.77 cm for uncontrolled structure. This value reduces to 3.5 cm, 2.96 cm and 2.46 cm by using several amount of control forces.

**Table 1.** The optimum results.

| Control limit | $K_p$ | $T_d$ | $T_i$ | $x_1$ (m) |
|---|---|---|---|---|
| 10% | -0.0168 | 0.3010 | 0.9086 | 0.0350 |
| 30% | -0.0185 | 1.0219 | 1.4020 | 0.0296 |
| 50% | -0.0544 | 0.6298 | 2.6096 | 0.0246 |

## 4. Discussion and Results

The optimum PID parameters were validated by using sets of near-fault ground excitation records. As presented in FEMA P695, the benchmark earthquake records with and without pulse were shown in Tables 2 and 3, respectively.

The maximum displacement, acceleration, control signal and force values for different levels of control force were presented in Tables 4-6 for records without pulse. The maximum displacement is 9.71 cm for uncontrolled structure. This maximum value occurs under fault parallel (FP) component of LA-Sepulveda VA record of 1994 Northridge earthquake. For this excitation, active control system is very effective. The maximum displacement reduces to 5.86 cm, 3.15cm and 2.59 cm by using 10%, 30% and 50% control force, respectively. For the structure with active tendon control, the critical excitation is the fault normal (FN) component of Cape Mendocino record of Cape Mendocino earthquake. By this excitation, the displacement, acceleration and control force plots are given as Figs. 3-5, respectively. As seen from the plots, the active control system is always effective in obtaining a quick damping. For the peak value of vibrations, reduction can be seen, but the reduction is significant for 30% and 50% control force. The reduction percentages of displacements are 16.28%, 38.08% and 50.77% for 10%, 30% and 50% control force, respectively. Although the optimization objective is the displacement of the structure, a significant effect on acceleration can be also

seen. For the other excitations with pulse, the maximum responses are presented as Tables 7-9. The critical excitation for structure with and without control is FP component of Sylmar-Olive View record of 1994 Northridge earthquake and the displacement, acceleration and control force plots are presented as Figs. 6-8, respectively. Similar conclusion of records without pulse can be also seen for records with pulse, but the active control system is more effective for the records with pulse since the optimization is done for a directivity pulse. In that case, the reduction percentages of maximum displacement under the critical excitation are 23.93%, 53.28% and 68.2% for 10%, 30% and 50% control force, respectively. As the conclusion, the control parameters optimized by using teaching learning- based optimization are robust under different types of near fault records.

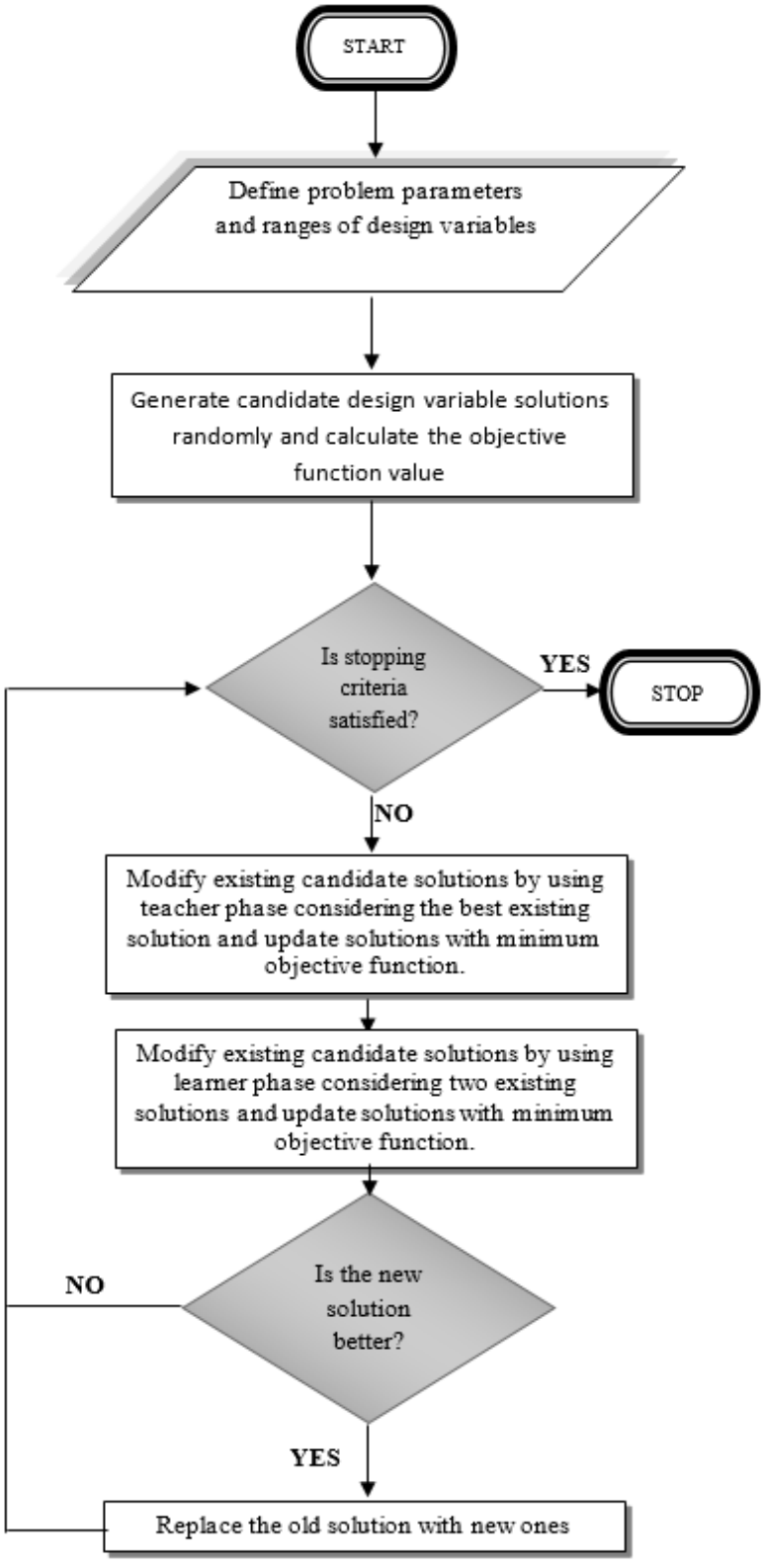


**Fig. 2.** Flowchart of the optimization process.

**Table 2.** Earthquake set for near-field excitations with pulses.

| Earthquake No. | Earthquake Name | Recording Station | Year | Magnitude |
|---|---|---|---|---|
| 1 | Irpinia, Italy-01 | Sturno | 1980 | 6.9 |
| 2 | Superstition Hills-02 | Parachute Test Site | 1987 | 6.5 |
| 3 | Duzce, Turkey | Duzce | 1999 | 7.1 |
| 4 | Erzican, Turkey | Erzican | 1992 | 6.7 |
| 5 | Imperial Valley-06 | El Centro Array #6 | 1979 | 6.5 |
| 6 | Imperial Valley-06 | El Centro Array #7 | 1979 | 6.5 |
| 7 | Kocaeli, Turkey | Izmit | 1999 | 7.5 |
| 8 | Landers | Lucerne | 1992 | 7.3 |
| 9 | Cape Mendocino | Petrolia | 1992 | 7.0 |
| 10 | Northridge-01 | 01 Rinaldi Receiving Sta | 1994 | 6.7 |
| 11 | Loma Prieta | Saratoga – Aloha | 1989 | 6.9 |
| 12 | Northridge-01 | 01 Sylmar – Olive View | 1994 | 6.7 |
| 13 | Chi-Chi, Taiwan | TCU065 | 1999 | 7.6 |
| 14 | Chi-Chi, Taiwan | TCU102 | 1999 | 7.6 |

**Table 3.** Earthquake set for near-field excitations without pulses.

| Earthquake No. | Earthquake Name | Recording Station | Year | Magnitude |
|---|---|---|---|---|
| 1 | Northridge-01 | LA - Sepulveda VA | 1994 | 6.7 |
| 2 | Loma Prieta | Bran | 1989 | 6.9 |
| 3 | Loma Prieta | Corralitos | 1989 | 6.9 |
| 4 | Cape Mendocino | Cape Mendocino | 1992 | 7.0 |
| 5 | Gazli, USSR | Karakyr | 1976 | 6.8 |
| 6 | Imperial Valley-06 | Bonds Corner | 1979 | 6.5 |
| 7 | Imperial Valley-06 | Chıhuahua | 1979 | 6.5 |
| 8 | Denali, Alaska | TAPS Pump Sta. #10 | 2002 | 7.9 |
| 9 | Nahanni, Canada | Site 1 | 1985 | 6.8 |
| 10 | Nahanni, Canada | Site 1 | 1985 | 6.8 |
| 11 | Northridge-01 | Northridge – Saticoy | 1994 | 6.7 |
| 12 | Chi-Chi, Taiwan | TCU067 | 1999 | 7.6 |
| 13 | Chi-Chi, Taiwan | TCU084 | 1999 | 7.6 |
| 14 | Kocaeli, Turkey | Yarimca | 1999 | 7.5 |

**Table 4.** The maximum responses of SDOF under near-fault ground motions without pulse (0.1 control force limit).

| EQ | CPNT | Displacement (cm) | | Acceleration (m/s$^2$) | | Control | | |
|---|---|---|---|---|---|---|---|---|
| | | Uncontrolled | Controlled | Uncontrolled | Controlled | Signal (cm) | Velocity (cm/s) | Force (kN) |
| 1 | FN | 4.29 | 2.41 | 20.40 | 11.92 | 0.23 | 5.60 | 2.75 |
| | FP | 9.71 | 5.86 | 46.17 | 29.87 | 0.64 | 14.1 | 7.65 |
| 2 | FN | 3.57 | 2.72 | 17.00 | 13.85 | 0.29 | 6.24 | 3.50 |
| | FP | 4.37 | 2.88 | 20.80 | 14.63 | 0.34 | 7.92 | 4.10 |
| 3 | FN | 5.96 | 4.42 | 28.32 | 22.63 | 0.50 | 11.6 | 6.07 |
| | FP | 3.33 | 1.90 | 15.82 | 9.65 | 0.23 | 6.24 | 2.76 |
| 4 | FN | 7.80 | 6.53 | 37.10 | 33.41 | 0.76 | 18.2 | 9.09 |
| | FP | 3.31 | 2.73 | 15.72 | 14.11 | 0.33 | 10.8 | 4.03 |
| 5 | FN | 4.75 | 3.11 | 22.60 | 15.83 | 0.32 | 7.78 | 3.86 |
| | FP | 3.82 | 2.15 | 18.18 | 11.00 | 0.22 | 5.37 | 2.70 |
| 6 | FN | 3.33 | 2.02 | 15.84 | 10.23 | 0.21 | 5.40 | 2.51 |
| | FP | 5.55 | 3.67 | 26.40 | 18.50 | 0.35 | 8.50 | 4.27 |
| 7 | FN | 1.83 | 1.57 | 8.72 | 8.05 | 0.18 | 4.35 | 2.20 |
| | FP | 1.69 | 1.14 | 8.05 | 5.78 | 0.11 | 2.81 | 1.34 |
| 8 | FN | 1.57 | 1.28 | 7.48 | 6.36 | 0.09 | 1.82 | 1.04 |
| | FP | 1.48 | 0.81 | 7.04 | 4.04 | 0.08 | 1.71 | 0.96 |
| 9 | FN | 4.70 | 2.71 | 22.36 | 13.79 | 0.31 | 6.85 | 3.68 |
| | FP | 4.17 | 2.42 | 19.83 | 12.43 | 0.25 | 6.35 | 3.01 |
| 10 | FN | 1.73 | 1.51 | 8.22 | 7.64 | 0.14 | 3.45 | 1.65 |
| | FP | 1.08 | 0.84 | 5.13 | 4.20 | 0.09 | 2.30 | 1.08 |
| 11 | FN | 2.83 | 1.76 | 13.45 | 8.92 | 0.17 | 4.57 | 2.00 |
| | FP | 3.71 | 2.01 | 17.65 | 10.08 | 0.21 | 4.18 | 2.48 |
| 12 | FN | 2.35 | 1.77 | 11.18 | 8.80 | 0.18 | 4.06 | 2.12 |
| | FP | 3.06 | 1.66 | 14.56 | 8.39 | 0.16 | 3.20 | 1.99 |
| 13 | FN | 4.45 | 3.10 | 21.16 | 15.44 | 0.27 | 5.70 | 3.29 |
| | FP | 2.89 | 2.21 | 13.74 | 11.26 | 0.23 | 5.40 | 2.76 |
| 14 | FN | 2.54 | 1.30 | 12.09 | 6.58 | 0.14 | 2.98 | 1.64 |
| | FP | 1.57 | 1.21 | 7.44 | 6.10 | 0.11 | 2.58 | 1.36 |

**Table 5.** The maximum responses of SDOF under near-fault ground motions without pulse (0.3 control force limit).

| EQ | CPNT | Displacement (cm) | | Acceleration (m/s²) | | Control | | |
|---|---|---|---|---|---|---|---|---|
| | | Uncontrolled | Controlled | Uncontrolled | Controlled | Signal (cm) | Velocity (cm/s) | Force (kN) |
| 1 | FN | 4.29 | 2.13 | 20.40 | 11.53 | 0.76 | 22.76 | 9.15 |
| | FP | 9.71 | 3.15 | 46.17 | 18.56 | 1.22 | 31.95 | 14.7 |
| 2 | FN | 3.57 | 1.52 | 17.00 | 8.80 | 0.51 | 14.41 | 6.10 |
| | FP | 4.37 | 1.64 | 20.80 | 9.39 | 0.64 | 17.81 | 7.71 |
| 3 | FN | 5.96 | 2.46 | 28.32 | 14.91 | 1.02 | 24.38 | 12.2 |
| | FP | 3.33 | 1.27 | 15.82 | 7.85 | 0.66 | 18.73 | 7.91 |
| 4 | FN | 7.80 | 4.83 | 37.10 | 28.90 | 2.05 | 56.57 | 24.7 |
| | FP | 3.31 | 1.72 | 15.72 | 11.34 | 0.90 | 32.18 | 10.9 |
| 5 | FN | 4.75 | 1.59 | 22.60 | 9.60 | 0.63 | 18.00 | 7.56 |
| | FP | 3.82 | 1.22 | 18.18 | 7.41 | 0.55 | 19.38 | 6.63 |
| 6 | FN | 3.33 | 1.33 | 15.84 | 8.39 | 0.54 | 15.89 | 6.56 |
| | FP | 5.55 | 2.70 | 26.40 | 15.30 | 1.01 | 28.22 | 12.1 |
| 7 | FN | 1.83 | 0.93 | 8.72 | 5.93 | 0.44 | 10.71 | 5.29 |
| | FP | 1.69 | 0.64 | 8.05 | 3.78 | 0.22 | 6.020 | 2.68 |
| 8 | FN | 1.57 | 1.07 | 7.48 | 5.95 | 0.29 | 5.610 | 3.54 |
| | FP | 1.48 | 0.06 | 7.04 | 3.31 | 0.21 | 4.080 | 2.47 |
| 9 | FN | 4.70 | 1.14 | 22.36 | 7.01 | 0.50 | 17.59 | 6.00 |
| | FP | 4.17 | 1.60 | 19.83 | 9.75 | 0.66 | 19.64 | 8.00 |
| 10 | FN | 1.73 | 0.96 | 8.22 | 5.55 | 0.32 | 8.040 | 3.81 |
| | FP | 1.08 | 0.59 | 5.13 | 3.26 | 0.21 | 8.120 | 2.52 |
| 11 | FN | 2.83 | 1.16 | 13.45 | 7.03 | 0.52 | 15.06 | 6.28 |
| | FP | 3.71 | 1.42 | 17.65 | 8.02 | 0.56 | 11.24 | 6.76 |
| 12 | FN | 2.35 | 1.42 | 11.18 | 7.63 | 0.37 | 8.420 | 4.43 |
| | FP | 3.06 | 1.14 | 14.56 | 6.41 | 0.40 | 7.210 | 4.82 |
| 13 | FN | 4.45 | 2.96 | 21.16 | 16.30 | 0.85 | 17.95 | 10.2 |
| | FP | 2.89 | 1.41 | 13.74 | 8.37 | 0.58 | 14.64 | 7.02 |
| 14 | FN | 2.54 | 0.78 | 12.09 | 4.49 | 0.30 | 7.470 | 3.67 |
| | FP | 1.57 | 0.87 | 7.44 | 4.81 | 0.26 | 6.870 | 3.12 |

**Table 6.** The maximum responses of SDOF under near-fault ground motions without pulse (0.5 control force limit).

| EQ | CPNT | Displacement (cm) | | Acceleration (m/s²) | | Control | | |
|---|---|---|---|---|---|---|---|---|
| | | Uncontrolled | Controlled | Uncontrolled | Controlled | Signal (cm) | Velocity (cm/s) | Force (kN) |
| 1 | FN | 4.29 | 1.80 | 20.40 | 10.97 | 1.25 | 38.13 | 15.1 |
| | FP | 9.71 | 2.59 | 46.17 | 18.80 | 1.75 | 53.84 | 21.1 |
| 2 | FN | 3.57 | 1.09 | 17.00 | 7.45 | 0.80 | 24.24 | 9.64 |
| | FP | 4.37 | 1.33 | 20.80 | 8.69 | 0.87 | 32.29 | 10.5 |
| 3 | FN | 5.96 | 1.64 | 28.32 | 11.17 | 1.13 | 28.16 | 13.6 |
| | FP | 3.33 | 0.99 | 15.82 | 7.54 | 0.96 | 27.70 | 11.6 |
| 4 | FN | 7.80 | 3.84 | 37.10 | 27.61 | 3.03 | 91.14 | 36.5 |
| | FP | 3.31 | 1.26 | 15.72 | 11.33 | 1.40 | 58.34 | 16.9 |
| 5 | FN | 4.75 | 1.19 | 22.60 | 9.25 | 0.96 | 30.59 | 11.5 |
| | FP | 3.82 | 0.94 | 18.18 | 7.89 | 0.95 | 34.30 | 11.4 |
| 6 | FN | 3.33 | 1.08 | 15.84 | 8.31 | 0.80 | 33.52 | 9.65 |
| | FP | 5.55 | 1.83 | 26.40 | 13.95 | 1.60 | 50.31 | 19.3 |
| 7 | FN | 1.83 | 0.60 | 8.72 | 4.77 | 0.53 | 14.81 | 6.33 |
| | FP | 1.69 | 0.48 | 8.05 | 2.87 | 0.30 | 8.850 | 3.66 |
| 8 | FN | 1.57 | 0.83 | 7.48 | 5.45 | 0.47 | 8.110 | 5.63 |
| | FP | 1.48 | 0.61 | 7.04 | 3.59 | 0.34 | 7.890 | 4.04 |
| 9 | FN | 4.70 | 0.83 | 22.36 | 6.67 | 0.77 | 35.52 | 9.23 |
| | FP | 4.17 | 1.28 | 19.83 | 9.66 | 1.06 | 33.56 | 12.8 |
| 10 | FN | 1.73 | 0.66 | 8.22 | 4.38 | 0.41 | 11.82 | 4.90 |
| | FP | 1.08 | 0.47 | 5.13 | 3.57 | 0.40 | 16.21 | 4.79 |
| 11 | FN | 2.83 | 0.86 | 13.45 | 7.28 | 0.83 | 23.90 | 10.0 |
| | FP | 3.71 | 1.20 | 17.65 | 8.63 | 0.77 | 22.58 | 9.30 |
| 12 | FN | 2.35 | 1.14 | 11.18 | 7.12 | 0.56 | 11.87 | 6.74 |
| | FP | 3.06 | 0.91 | 14.56 | 6.21 | 0.56 | 10.69 | 6.68 |
| 13 | FN | 4.45 | 2.64 | 21.16 | 16.53 | 1.14 | 29.26 | 13.7 |
| | FP | 2.89 | 1.02 | 13.74 | 6.49 | 0.81 | 24.80 | 9.76 |
| 14 | FN | 2.54 | 0.64 | 12.09 | 4.19 | 0.42 | 11.25 | 5.10 |
| | FP | 1.57 | 0.74 | 7.44 | 4.54 | 0.38 | 11.60 | 4.53 |

The structural reactions of the single degree of freedom system under the effect of the earthquake records without 28 pulse vibrations are given in Tables 2-4 for the control limit 0.1, 0.3 and 0.5, respectively. The maximum displacement and total acceleration of the uncontrolled structure is 9.71 cm and 46.17 m/s² under FP component of EQ 2. In case with a control limit 0.1, the maximum displacement and total acceleration of the single degree of freedom system reduce to 6.53 cm and 33.41 m/s² under FN component of EQ 4. There is a significant reduction in the displacement and acceleration of all records. These reduction percentages are between 12.72% under FN Component of EQ 10 and 48.82% under FN component of EQ 14 in the displacement and between 7.05% under FN Component of EQ 10 and 45.57% under FN component of EQ 14 in the total acceleration. In addition, the maximum control signal and the control force are 0.76 cm and 9.09 kN under FN component of EQ 4, respectively. In the second case with a control limit 0.3, the maximum displacement and total acceleration of the single degree of freedom system reduce to 4.83 cm and 28.90 m/s² under FN component of EQ 4. The displacement and total acceleration values decreased by 26% and 13.50% compared to the previous situation but the required control force increased by 63.25%. In the last case with a control limit 0.5, the maximum displacement and total acceleration of the uncontrolled single degree of freedom system decreased to 3.84 cm and 27.61 m/s² with the increase of the control force limit under all records. As a result, a percentage decrease in displacement and acceleration value of 60.45% and 40.20% occurred, respectively. The required control force is 36.51 kN.

The structural reactions of the single degree of freedom system under the effect of the earthquake records with 28 pulse vibrations are given in Tables 7-9 for the control limit 0.1, 0.3 and 0.5, respectively. The maximum displacement and total acceleration of the uncontrolled structure is 6.12 cm and 29.12 m/s² under FP component of EQ 10. In case with a control limit 0.1, the maximum displacement and total acceleration of the single degree of freedom system reduce to 4.64 cm and 23.29 m/s² under FP component of EQ 12. There is a significant reduction in the displacement and acceleration of all records except FP component of EQ 6 in the total acceleration. This reduction percentages are between 3.64% under FP Component of EQ 6 and 48.06% under FN component of EQ 1 in the displacement and between 2.98% under FP Component of EQ 7 and 43.94% under FN component of EQ 14 in the total acceleration. In addition, the maximum control signal and the control force are 0.42 cm and 5.04 kN under FP component of EQ 12, respectively. In the second case with a control limit 0.3, the maximum displacement and total acceleration of the single degree of freedom system reduce to 2.85 cm and 16.00 m/s² under FP component of EQ 12. The displacement and total acceleration values decreased by 38.58% and 31.30% compared to the previous situation but the required control force increased by 56.55%. In the last case with a control limit 0.5, the maximum displacement and total acceleration of the uncontrolled single degree of freedom system decreased to 1.94 cm and 12.18 m/s² with the increase of the control force limit under all records. As a result, a percentage decrease in displacement and acceleration value of 68.30% and 58.17% occurred, respectively. The required control force is 14.8 kN.

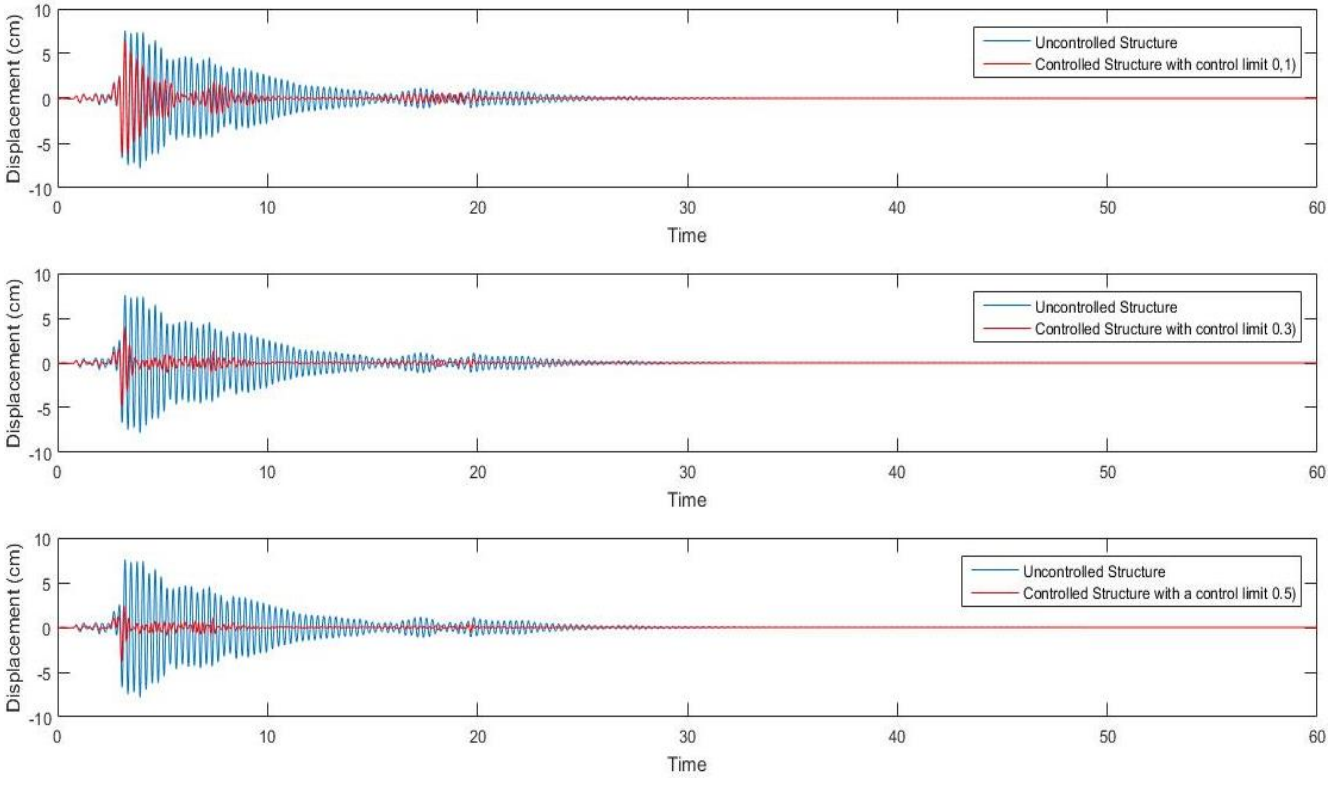


**Fig. 3.** Displacement time history of controlled and uncontrolled SDOF under Cape Mendocino, Cape Mendocino - FN component.

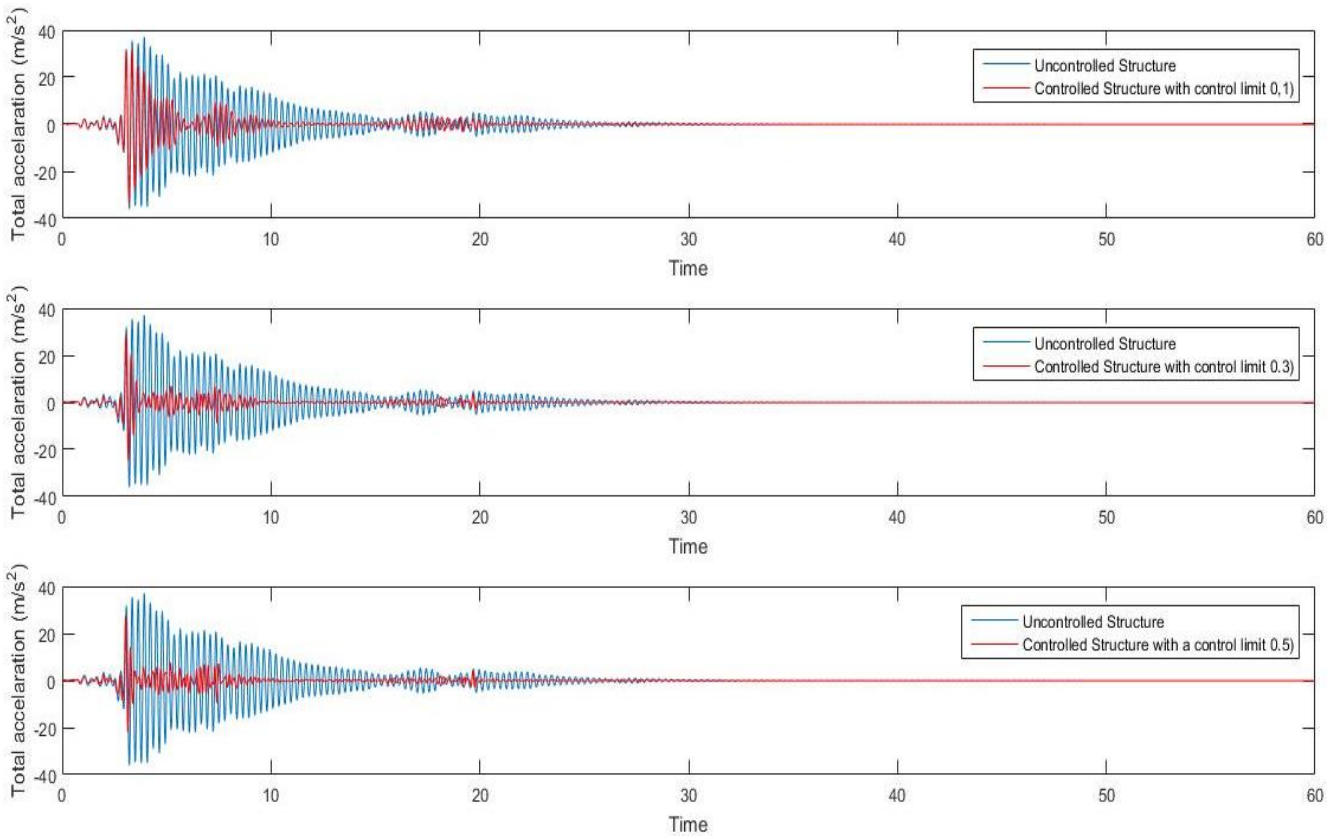


**Fig. 4.** Total acceleration time history of controlled and uncontrolled SDOF under Cape Mendocino, Cape Mendocino - FN component.

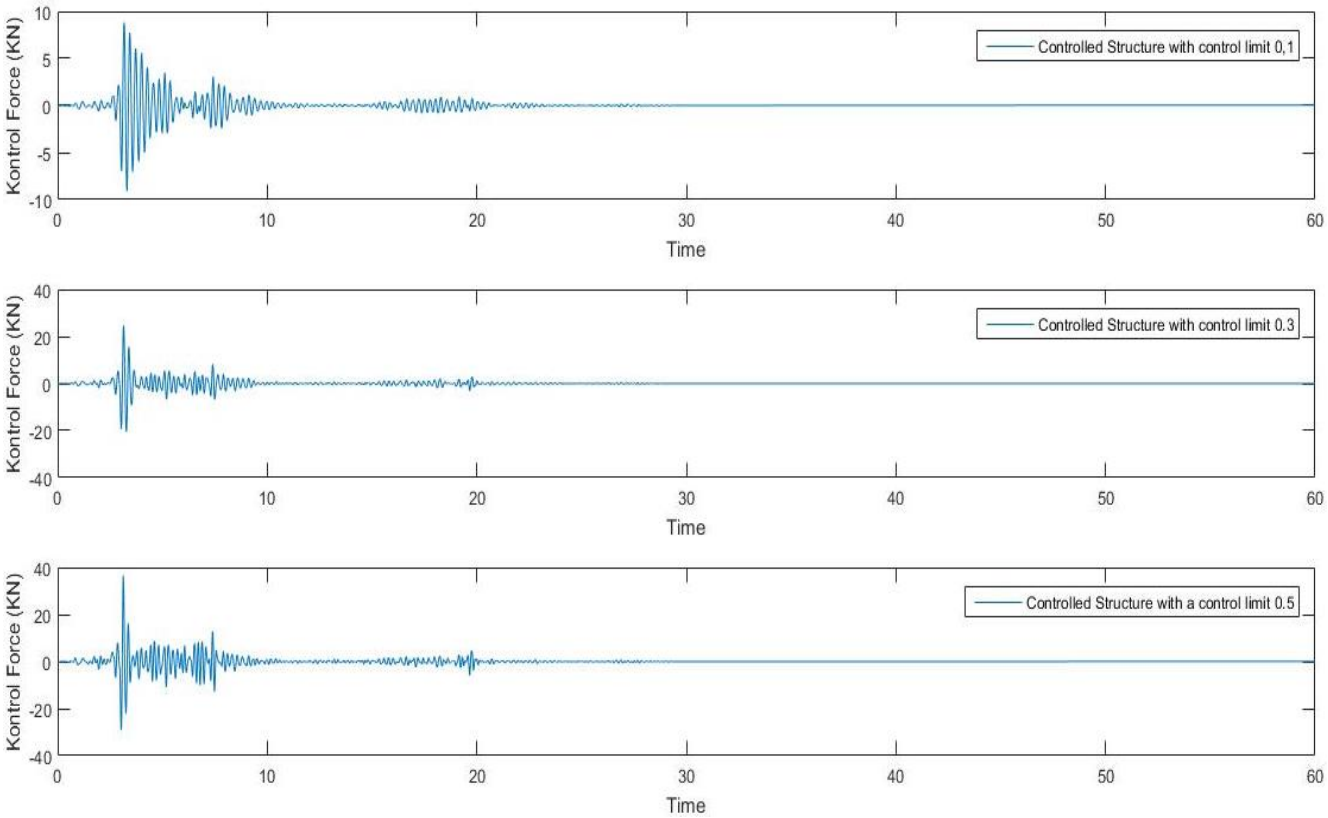


**Fig. 5.** Control force time history of controlled and uncontrolled SDOF under Cape Mendocino, Cape Mendocino - FN component.

**Table 7.** The maximum responses of SDOF under near-fault ground motions with pulse (0.1 control force limit).

| EQ | CPNT | Displacement (cm) | | Acceleration (m/s²) | | Control | | |
|---|---|---|---|---|---|---|---|---|
| | | Uncontrolled | Controlled | Uncontrolled | Controlled | Signal (cm) | Velocity (cm/s) | Force (kN) |
| 1 | FN | 2.33 | 1.21 | 11.06 | 6.20 | 0.13 | 2.79 | 1.61 |
| | FP | 3.50 | 1.92 | 16.66 | 9.77 | 0.20 | 4.69 | 2.39 |
| 2 | FN | 3.74 | 2.39 | 17.76 | 12.00 | 0.20 | 4.44 | 2.39 |
| | FP | 2.72 | 1.75 | 12.94 | 8.91 | 0.18 | 4.05 | 2.21 |
| 3 | FN | 3.23 | 2.30 | 15.35 | 11.61 | 0.21 | 4.38 | 2.59 |
| | FP | 2.55 | 2.18 | 12.14 | 11.00 | 0.20 | 3.92 | 2.41 |
| 4 | FN | 4.32 | 2.95 | 20.53 | 15.04 | 0.30 | 7.23 | 3.58 |
| | FP | 2.31 | 1.82 | 11.00 | 9.05 | 0.15 | 3.23 | 1.77 |
| 5 | FN | 2.07 | 1.58 | 9.85 | 8.00 | 0.15 | 3.15 | 1.77 |
| | FP | 2.65 | 1.64 | 12.61 | 8.34 | 0.18 | 4.45 | 2.18 |
| 6 | FN | 2.11 | 1.51 | 10.01 | 7.55 | 0.15 | 3.02 | 1.86 |
| | FP | 1.65 | 1.59 | 7.84 | 7.89 | 0.10 | 1.77 | 1.19 |
| 7 | FN | 3.02 | 2.27 | 14.37 | 11.62 | 0.26 | 5.71 | 3.12 |
| | FP | 1.69 | 1.52 | 8.05 | 7.81 | 0.18 | 4.00 | 2.14 |
| 8 | FN | 3.43 | 2.68 | 16.31 | 13.74 | 0.32 | 8.75 | 3.86 |
| | FP | 2.53 | 2.02 | 12.00 | 10.51 | 0.24 | 7.90 | 2.95 |
| 9 | FN | 3.33 | 1.82 | 15.85 | 9.27 | 0.21 | 4.75 | 2.58 |
| | FP | 2.86 | 2.22 | 13.58 | 11.26 | 0.24 | 5.18 | 2.83 |
| 10 | FN | 4.32 | 3.49 | 20.54 | 17.40 | 0.33 | 7.86 | 3.97 |
| | FP | 6.12 | 3.63 | 29.12 | 18.45 | 0.38 | 8.81 | 4.52 |
| 11 | FN | 2.88 | 1.72 | 13.70 | 8.76 | 0.20 | 4.60 | 2.41 |
| | FP | 1.15 | 0.89 | 5.46 | 4.48 | 0.11 | 2.77 | 1.34 |
| 12 | FN | 2.54 | 1.84 | 12.08 | 9.12 | 0.18 | 3.60 | 2.14 |
| | FP | 6.10 | 4.64 | 29.00 | 23.29 | 0.42 | 8.30 | 5.04 |
| 13 | FN | 3.63 | 2.51 | 17.26 | 12.62 | 0.25 | 5.78 | 3.03 |
| | FP | 2.85 | 1.70 | 13.54 | 8.46 | 0.16 | 3.26 | 1.87 |
| 14 | FN | 1.07 | 0.74 | 5.08 | 3.66 | 0.05 | 1.01 | 0.56 |
| | FP | 0.91 | 0.61 | 4.31 | 3.08 | 0.06 | 1.22 | 0.65 |

**Table 8.** The maximum responses of SDOF under near-fault ground motions with pulse (0.3 control force limit).

| EQ | CPNT | Displacement (cm) | | Acceleration (m/s²) | | Control | | |
|---|---|---|---|---|---|---|---|---|
| | | Uncontrolled | Controlled | Uncontrolled | Controlled | Signal (cm) | Velocity (cm/s) | Force (kN) |
| 1 | FN | 2.33 | 0.82 | 11.06 | 4.72 | 0.32 | 6.52 | 3.86 |
| | FP | 3.50 | 1.12 | 16.66 | 6.87 | 0.46 | 13.4 | 5.54 |
| 2 | FN | 3.74 | 1.37 | 17.76 | 7.61 | 0.33 | 8.40 | 3.91 |
| | FP | 2.72 | 1.17 | 12.94 | 6.86 | 0.46 | 11.9 | 5.57 |
| 3 | FN | 3.23 | 1.21 | 15.35 | 7.01 | 0.42 | 9.91 | 5.11 |
| | FP | 2.55 | 1.64 | 12.14 | 9.40 | 0.63 | 14.6 | 7.61 |
| 4 | FN | 4.32 | 1.80 | 20.53 | 10.98 | 0.72 | 18.4 | 8.73 |
| | FP | 2.31 | 1.49 | 11.00 | 8.08 | 0.31 | 8.14 | 3.78 |
| 5 | FN | 2.07 | 1.06 | 9.85 | 6.21 | 0.38 | 9.06 | 4.53 |
| | FP | 2.65 | 1.09 | 12.61 | 6.23 | 0.42 | 10.9 | 5.08 |
| 6 | FN | 2.11 | 0.95 | 10.01 | 5.15 | 0.30 | 7.01 | 3.62 |
| | FP | 1.65 | 1.33 | 7.84 | 7.20 | 0.30 | 5.45 | 3.57 |
| 7 | FN | 3.02 | 0.98 | 14.37 | 6.00 | 0.43 | 9.57 | 5.16 |
| | FP | 1.69 | 0.64 | 8.05 | 3.95 | 0.29 | 7.00 | 3.51 |
| 8 | FN | 3.43 | 1.47 | 16.31 | 9.57 | 0.71 | 25.3 | 8.52 |
| | FP | 2.53 | 1.23 | 12.00 | 7.48 | 0.57 | 23.7 | 6.92 |
| 9 | FN | 3.33 | 1.39 | 15.85 | 7.98 | 0.42 | 14.8 | 5.06 |
| | FP | 2.86 | 1.34 | 13.58 | 7.16 | 0.41 | 11.2 | 4.91 |
| 10 | FN | 4.32 | 2.66 | 20.54 | 14.84 | 0.83 | 19.8 | 10.0 |
| | FP | 6.12 | 1.91 | 29.12 | 11.57 | 0.80 | 18.7 | 9.67 |
| 11 | FN | 2.88 | 1.16 | 13.70 | 6.91 | 0.44 | 14.0 | 5.28 |
| | FP | 1.15 | 0.93 | 5.46 | 5.77 | 0.47 | 12.5 | 5.60 |
| 12 | FN | 2.54 | 1.48 | 12.08 | 7.80 | 0.44 | 9.27 | 5.33 |
| | FP | 6.10 | 2.85 | 29.00 | 16.00 | 0.96 | 18.8 | 11.6 |
| 13 | FN | 3.63 | 1.83 | 17.26 | 10.35 | 0.64 | 15.8 | 7.72 |
| | FP | 2.85 | 1.45 | 13.54 | 7.96 | 0.37 | 8.57 | 4.49 |
| 14 | FN | 1.07 | 0.66 | 5.08 | 3.34 | 0.13 | 2.54 | 1.58 |
| | FP | 0.91 | 0.46 | 4.31 | 2.46 | 0.13 | 2.79 | 1.62 |

**Table 9.** The maximum responses of SDOF under near-fault ground motions with pulse (0.5 control force limit).

| EQ | CPNT | Displacement (cm) | | Acceleration (m/s²) | | Control | | |
|---|---|---|---|---|---|---|---|---|
| | | Uncontrolled | Controlled | Uncontrolled | Controlled | Signal (cm) | Velocity (cm/s) | Force (kN) |
| 1 | FN | 2.33 | 0.63 | 11.06 | 4.55 | 0.41 | 12.46 | 4.93 |
| | FP | 3.50 | 0.92 | 16.66 | 7.64 | 0.91 | 28.16 | 11.0 |
| 2 | FN | 3.74 | 1.17 | 17.76 | 7.70 | 0.59 | 14.46 | 7.06 |
| | FP | 2.72 | 0.89 | 12.94 | 5.94 | 0.60 | 17.30 | 7.25 |
| 3 | FN | 3.23 | 0.85 | 15.35 | 5.64 | 0.55 | 13.60 | 6.60 |
| | FP | 2.55 | 1.36 | 12.14 | 8.76 | 0.81 | 21.49 | 9.80 |
| 4 | FN | 4.32 | 1.33 | 20.53 | 10.43 | 1.14 | 28.48 | 13.7 |
| | FP | 2.31 | 1.26 | 11.00 | 7.79 | 0.53 | 11.89 | 6.36 |
| 5 | FN | 2.07 | 0.72 | 9.85 | 5.00 | 0.46 | 17.94 | 5.52 |
| | FP | 2.65 | 0.93 | 12.61 | 5.38 | 0.52 | 17.33 | 6.24 |
| 6 | FN | 2.11 | 0.74 | 10.01 | 4.26 | 0.43 | 10.97 | 5.12 |
| | FP | 1.65 | 1.09 | 7.84 | 6.76 | 0.49 | 8.660 | 5.95 |
| 7 | FN | 3.02 | 0.61 | 14.37 | 4.42 | 0.48 | 14.23 | 5.82 |
| | FP | 1.69 | 0.42 | 8.05 | 3.05 | 0.33 | 8.750 | 3.92 |
| 8 | FN | 3.43 | 1.11 | 16.31 | 8.33 | 1.05 | 38.10 | 12.7 |
| | FP | 2.53 | 0.86 | 12.00 | 8.32 | 1.08 | 40.13 | 13.0 |
| 9 | FN | 3.33 | 1.20 | 15.85 | 8.10 | 0.60 | 24.63 | 7.17 |
| | FP | 2.86 | 1.34 | 13.58 | 8.48 | 0.66 | 23.23 | 7.91 |
| 10 | FN | 4.32 | 2.09 | 20.54 | 13.76 | 1.18 | 32.55 | 14.2 |
| | FP | 6.12 | 1.27 | 29.12 | 9.82 | 1.11 | 27.57 | 13.3 |
| 11 | FN | 2.88 | 1.06 | 13.70 | 7.46 | 0.75 | 23.38 | 9.08 |
| | FP | 1.15 | 0.86 | 5.460 | 6.60 | 0.79 | 25.97 | 9.54 |
| 12 | FN | 2.54 | 1.12 | 12.08 | 6.67 | 0.69 | 17.62 | 8.36 |
| | FP | 6.10 | 1.94 | 29.00 | 12.18 | 1.23 | 29.00 | 14.8 |
| 13 | FN | 3.63 | 1.64 | 17.26 | 10.74 | 1.00 | 26.86 | 12.0 |
| | FP | 2.85 | 1.29 | 13.54 | 8.09 | 0.58 | 17.36 | 7.02 |
| 14 | FN | 1.07 | 0.59 | 5.08 | 3.15 | 0.21 | 3.570 | 2.52 |
| | FP | 0.91 | 0.38 | 4.31 | 2.29 | 0.18 | 3.740 | 2.21 |

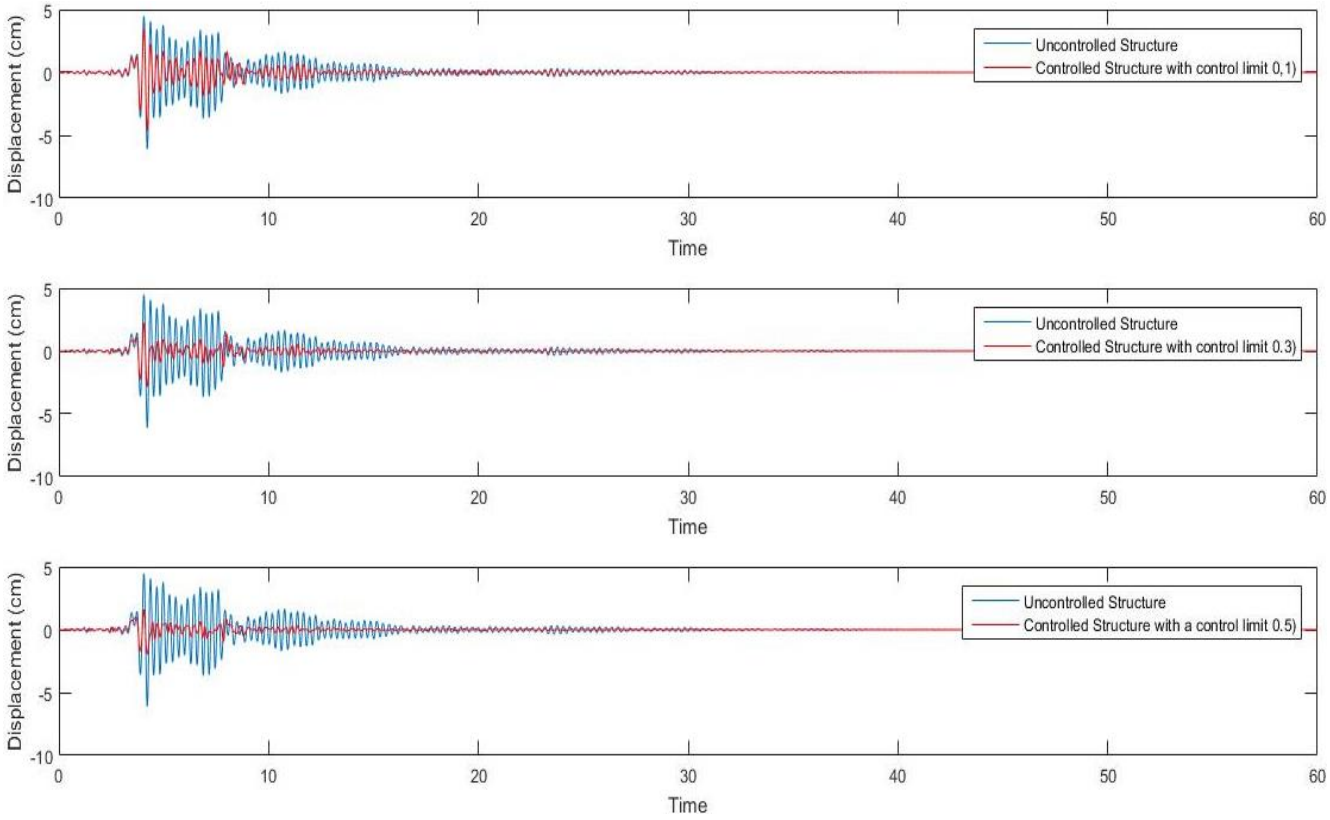


**Fig. 6.** Displacement time history of controlled and uncontrolled SDOF under Northridge-01, 01 Sylmar - Olive View- FP component.

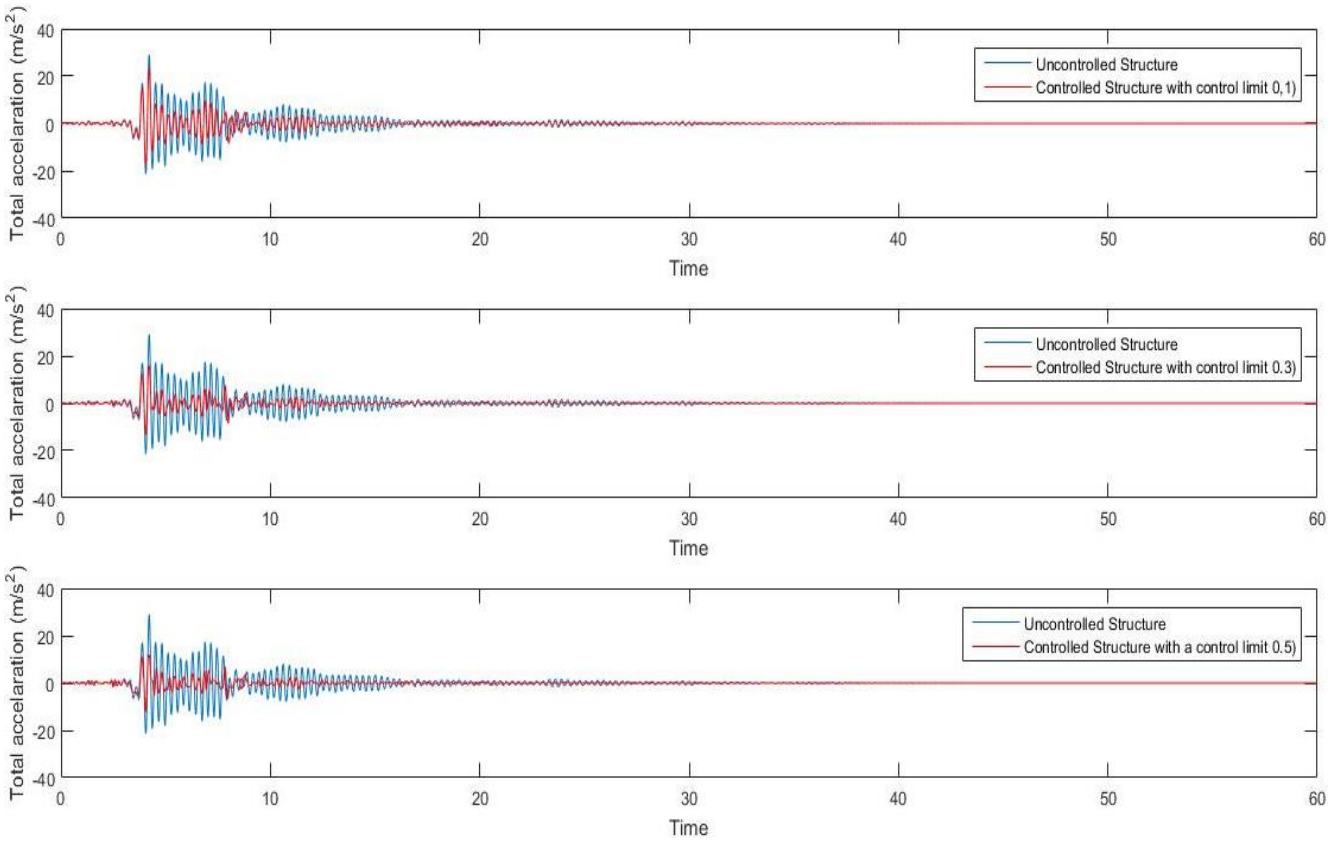


**Fig. 7.** Total acceleration time history of controlled and uncontrolled SDOF under Northridge-01, 01 Sylmar - Olive View- FP component.

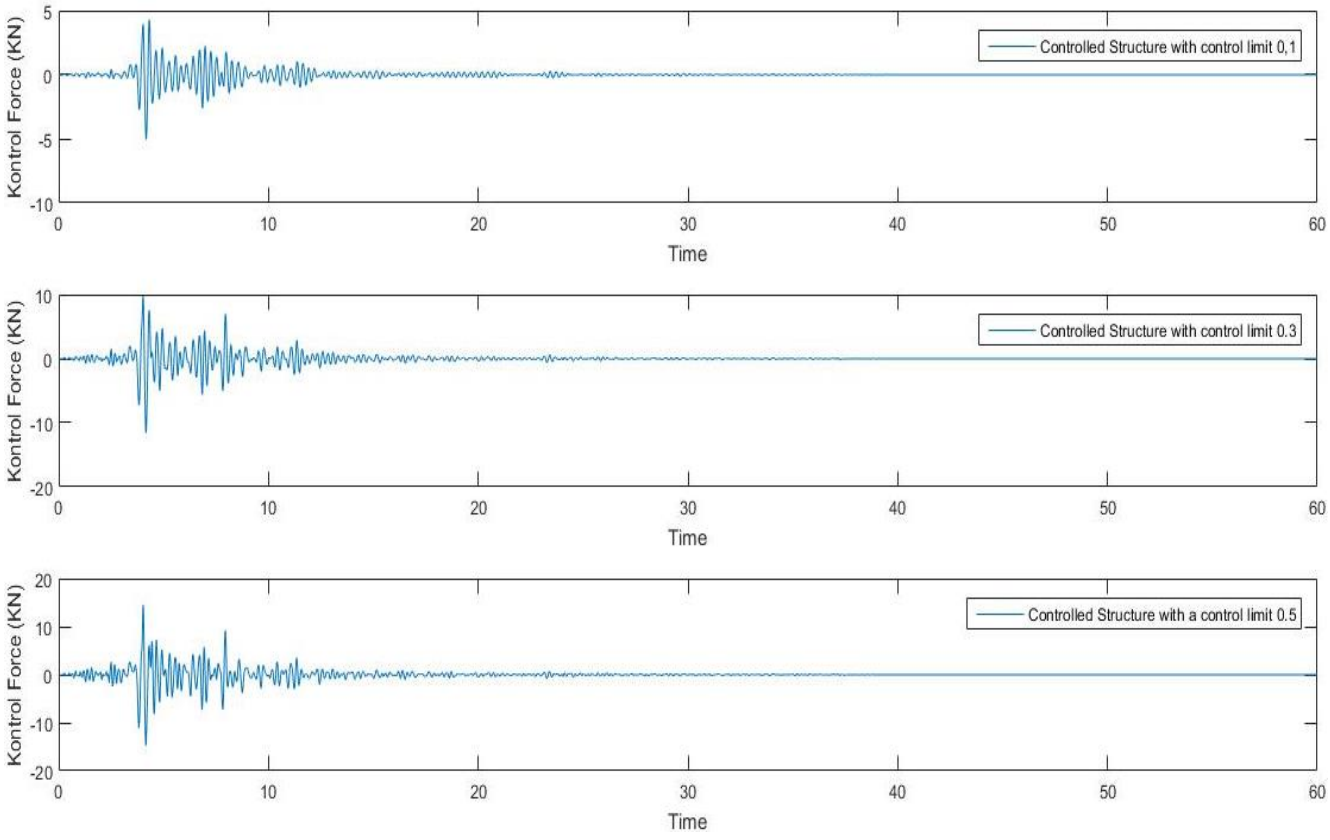


**Fig. 8.** The control force time history of controlled and uncontrolled SDOF under Northridge-01, 01 Sylmar - Olive View- FP component.

## 5. Conclusions

In this study, active structural control on single degree of freedom structures using teaching learning based algorithm are proposed. The conclusions about these structures with optimized PID are as follows:

- The optimum PID parameters were calculated in a short time using teaching learning based algorithm.
- The behavior of single degree of freedom structures with different control limits was examined under 56 earthquake recordings, not a few earthquake recordings, and structural reactions were significantly reduced in all records.
- The effects of the control force on single degree of freedom structures were examined carefully and it was determined that the generated control force was actually applicable.

## REFERENCES


Aldemir U, Bakioglu M (2001). Active structural control based on the prediction and degree of stability. *Journal of Sound and Vibration*, 247(4), 561-576.

Amini F, Samani MZ (2014). A wavelet-based adaptive pole assignment method for structural control. *Computer-Aided Civil and Infrastructure Engineering*, 29(6), 464-477.

Bakule L, Rehák B, Papík M (2016). Decentralized networked control of building structures. *Computer-Aided Civil and Infrastructure Engineering*, 31(11), 871-886.

Bitaraf M, Hurlebaus S, Barroso, LR (2012). Active and semi-active adaptive control for undamaged and damaged building structures under seismic load. *Computer-Aided Civil and Infrastructure Engineering*, 27(1), 48-64.

Chang CC, Lin CC (2009). H∞ drift control of time-delayed seismic structures. *Earthquake Engineering and Engineering Vibration*, 8(4), 617-626.

Lin CC, Chang CC, Wang JF (2010). Active control of irregular buildings considering soil–structure interaction effects. *Soil Dynamics and Earthquake Engineering*, 30(3), 98-109.

Makris N (1997). Rigidity–plasticity–viscosity: Can electrorheological dampers protect base-isolated structures from near-source ground motions? *Earthquake Engineering & Structural Dynamics*, 26(5), 571-591.

Nazarimofrad E, Zahrai SM (2017). Fuzzy control of asymmetric plan buildings with active tuned mass damper considering soil-structure interaction. *Soil Dynamics and Earthquake Engineering*, 115, 838-852

Nigdeli SM, Boduroğlu MH (2013). Active tendon control of torsionally irregular structures under near-fault ground motion excitation. *Computer-Aided Civil and Infrastructure Engineering*, 28(9), 718-736.

Nigdeli SM, Boduroğlu MH (2014). Robustness against Time Delay and Control Force Capacity for Torsionally Irregular Active Controlled Structures. *5th European Conference of Civil Engineering* (ECCIE'14), Florence, Italy.

Rao RV, Savsani VJ, Vakharia DP (2011). Teaching–learning-based optimization: a novel method for constrained mechanical design optimization problems. *Computer-Aided Design*, 43(3), 303-315.

Ulusoy S, Nigdeli SM, Bekdas G. (2018). Time delay factor of structural control systems for excitations with and without pulses. *International Journal of Theoretical and Applied Mechanics*, 3, 74-81.

Wang N, Adeli H (2015). Self-constructing wavelet neural network algorithm for nonlinear control of large structures. *Engineering Applications of Artificial Intelligence*, 41, 249-258.

Wu JC, Yang JN, Agrawal AK (1998). Applications of sliding mode control to benchmark problems. *Earthquake Engineering & Structural Dynamics*, 27(11), 1247-1265

Yang JN, Wu JC, Agrawal AK, Hsu SY (1997). Sliding mode control with compensator for wind and seismic response control. *Earthquake Engineering & Structural Dynamics*, 26(11), 1137-1156.

Challenge Journal of Structural Mechanics

Research Article

# Comparison of equivalent seismic load and response spectrum methods according to TSC 2018 and TSC 2007

İbrahim Hakkı Erkan *, Talha Polat Doğan

*Department of Civil Engineering, Konya Technical University, 42075 Konya, Turkey*

**ABSTRACT**

In this study, two different analysis methods were compared; the first is a linear static analysis method and the second is a linear dynamic analysis method. First one is the Equivalent Seismic Load Method, which is a linear static method where seismic loads can be obtained by applying a simple calculation. The second method, the Response Spectrum method, is a linear dynamic analysis method which obtains the seismic loads using more complex statistical calculations. For this analysis study, 18 structural models with 3 different building heights were analyzed according to the conditions of Equivalent Seismic Load Method and Response Spectrum Method specified in both TSC 2007 and TSC 2018 and base shear forces obtained as a result of these analyzes were compared. As a result of analysis; compared to the results obtained from TSC 2007, due to the effective stiffness coefficients specified in TSC 2018, it was observed that the base shear forces obtained for both methods were lower and the modal period values were longer in the analyzes applied according to TSC 2018. This means that the structural systems created with the designs according to TSC 2018 are more ductile than the structural systems created with the designs made according to TSC 2007. Base shear forces obtained by 2 different analysis methods applied according to regulations stated in both TSC 2018 and TSC 2007; it was observed that the base shear forces obtained by the Equivalent Seismic Load Method were higher than the results of the Response Spectrum Method.

**ARTICLE INFO**

*Article history:*
Received 25 August 2019
Revised 23 October 2019
Accepted 4 November 2019

*Keywords:*
Equivalent seismic load method
Response spectrum method
Effective stiffness coefficient
Base shear
Modal analysis

## 1. Introduction

There are various regulations and standards around the world in order to ensure the adequacy of the structures to be constructed under the titles of inspection, usability and safety. In these regulations and standards, there are various solution methods for the design of structures and alternative solutions that can be used in exceptional cases where these solution methods cannot be applied effectively. While some of these calculation and analysis methods are highly complex and developed directly on the goal of predicting the actual performance of the building, some methods provide simpler solutions to ensure adequate security of structures. The reason that these solutions are simple, that is to say less complicated, is that some assumptions are used in the calculations and the use of safety factors. Examples of these safety factors are reducing the material strength, increasing the loads expected to be effected, reducing the effective rigidities of the structural system elements and accepting the ground bearing capacity as low.

Seismic loading is one of the most important topics to consider in the design of structures. When it comes to these effects, it must remembered that our country is located on an active fault map. Today, population density is generally found in the areas close to these fault zones. Throughout history, the result of seismic movements, our country experienced heavy losses of life and property as well as moral damage on the population and the economy. For this reason, it is known that the real behavior of the existing buildings and the buildings to be constructed under seismic effects in our country can be determined

* *Corresponding author*. Tel.: +90-332-223-8818 ; Fax: +90-332-241-0635 ; E-mail address: iherkan@ktun.edu.tr (İ. H. Erkan)
ISSN: 2149-8024 / DOI: https://doi.org/10.20528/cjsmec.2019.04.003

with the nonlinear analysis. However, it is of utmost importance that the structural strength of the buildings against seismic effects is meticulously and accurately determined even by linear calculations that specified by the regulations.

Considering these situations, an analysis study was conducted to examine the results of Equivalent Seismic Load Analysis and Response Spectrum Analysis, which are used to estimate seismic loads that are predicted to be met by structures as linear analysis methods according to regulations. These analyzes were carried out in accordance with the conditions stated in TSC 2007 and TSC 2018.

In the literature, Yılmaz (2008) applied linear analysis according to TSC 2007, Equivalent Seismic Load Method to form the initial step of the nonlinear analysis to determine the seismic performance of an existing building. Uzun (2014) conducted an analysis study to examine the effect of desired slab type on the seismic performance of a thirty-three-storey building and used the Response Spectrum Method in the initial step of this study as linear analysis. Pakoglu (2009) in his thesis study on a 100 meter high, reinforced concrete (RC) tube walled structural system has preferred and Response Spectrum Method has used to determine the linear seismic loads. Kıran (2010) preferred to use the Equivalent Seismic Load Method in his study in order to examine the behavior of an existing 8-storey building and a newly designed 2-storey building under the effects of seismic effects. Dinçer et al. (2014) carried out the performance analysis of a 4-storey school building with static push over analysis and preferred to make the calculation according to the Response Spectrum Method in the linear analysis section which is the initial step of this analysis study. Köse (2008) designed a 3-storey reinforced concrete structure in her thesis and chose to use the Equivalent Seismic Load Method in his study in order to investigate the behavior of this structure under seismic effects. Arias et al. (2019) ASCE / SEI 7-10 / 2010 in their study according to the seismic effects of multi-degree of freedom systems in their work in order to examine the interaction of the structure of the soil in their study carried out with the method of Response Spectrum Analysis. Kocer et al. (2018) presented a comparative analysis of the design considerations specified in the TSC 2018 and TSC 2007 regulations on the seismic data selected for 4 different provinces in their analytical study in order to compare the linear calculation methods. In the study of Erkan et al. (2019) conducted an analytical study to investigate the effect of the change in the ratio of reinforced concrete walls on seismic performance. In this study, Equivalent Seismic Load Analysis method was preferred. Doğan (2019), in his thesis study, evaluated the building models he prepared to examine seismic performances according to TSC 2007 and TSC 2018 and made a comparison in accordance with the conditions specified for Equivalent Seismic Load Method and Response Spectrum Method specified in these regulations. Arslan et al. (2013) examined the characteristics of the earthquake that occurred in Kütahya in 2011 in their study.

## 2. Material and Method

### *2.1. Determination of geometric properties of analysis models*

Within the scope of the study, there are 3 different building heights including 4-storey, 7-storey and 10-storey; 1 reference model and 5 RC walled models are designed. For each building height, 6 models were prepared and a total of 18 types were created. The models containing the reinforced concrete walls were prepared by using different amount of RC walls up to the ratio value (the ratio of the sum of the RC wall areas in a floor plan in any direction to the total of the floor plan areas of the structure is equal to or greater than 0.002 (TBDY, 2018), which defines the structures consisting of the reinforced concrete walled structural system specified in TSC 2018. Naming of the prepared building models was made as 'Model (number of storey).(number of RC wall ratio)'. For example, a building model with a 7-storey and 4th wall ratio is called 'Model 7.4', and the model that provides 4-storey and 1st Wall ratio is called 'Model 4.1'. In Table 1, the RC wall ratios were determined according to the conditions specified in TSC 2018 that are given for different building heights. According to these values, this ratio is calculated as 0 because there is no reinforced concrete wall in the floor plans of the building models with the 1st RC wall ratio for each building height.

According to TSC 2018, the response modification coefficients of these models are taken as $R$=8 and the over strength factors as $D$=3. Models with a RC wall ratio number from 2 to 5, the structural system conforms to the definition of structures consisting of both reinforced concrete walls and frames with high ductility according to TSC 2018. The response modification coefficients of these models are taken as $R$=7 and over strength factors as $D$=2.5. The structural system of the models with the RC wall ratio number 6 complies with the definition of structures made of reinforced RC walls with high ductility. The response modification coefficients of these models are taken as R = 6 and over strength factors as $D$=2.5.

**Table 1.** Ratio of reinforced concrete walls determined for analysis models.

| Number of RC wall ratio | 4 Storey | 7 Storey | 10 Storey |
|---|---|---|---|
| 1 | 0 | 0 | 0 |
| 2 | 0.512 | 0.512 | 0.512 |
| 3 | 1.007 | 1.011 | 1.007 |
| 4 | 1.416 | 1.416 | 1.416 |
| 5 | 1.700 | 1.702 | 1.709 |
| 6 | 2.016 | 2.023 | 2.014 |

The models have 8 bays in X and Y directions and the length of each bay is 4 meters. Rigid diaphragm was adopted and beamed slab type was preferred. The slab

thickness used in the buildings was determined as 15 cm. In all models, the columns are 40 x 40 cm and the beams are 25 x 50 cm. The dimensions of reinforced concrete wall elements vary according to the type of construction model designed to meet the selected wall ratio. The dimensions of the RC walls used in the models are given in Table 2.

**Table 2.** Dimensions of reinforced concrete walls determined for analysis models.

| Number of RC wall ratio | 4 Storey | 7 Storey | 10 Storey |
|---|---|---|---|
| 1 | 0 | 0 | 0 |
| 2 | 210 x 25 cm | 210 x 25 cm | 210 x 25 cm |
| 3 | 275 x 25 cm | 290 x 25 cm | 275 x 25 cm |
| 4 | 290 x 25 cm | 290 x 25 cm | 290 x 25 cm |
| 5 | 290 x 25 cm | 305 x 25 cm | 280 x 25 cm |
| 6 | 295 x 25 cm | 290 x 25 cm | 275 x 25 cm |

In TSC 2018, effective rigidity multipliers are defined on columns, beams and RC wall elements in order to be able to make modeling in accordance with the Design by Strength. There is no such requirement in TSC 2007. The structural elements of the structural system are defined according to the Mander Confined Concrete Theorem from the Section Designer menu on the SAP2000 analyzing software. As the dimensions of the structural system elements except the RC walls are the same in all construction models, the reinforcement is determined to be uniform for all models. The reinforcement determined for each section of wall was calculated separately up to the $H_{CR}$ as well as the height of the building. This table also shows the lengths of the flange and web regions of the RC wall elements. The models designed in this way have been subjected to the analysis procedures with Equivalent Seismic Load Method and Response Spectrum Method according to TSC 2018 and TSC 2007. The analyses performed due to the effective rigidity multipliers defined on the structural system elements were carried out separately for each regulation. Structural plans of the models created in accordance with the given data are shown in Fig. 1.

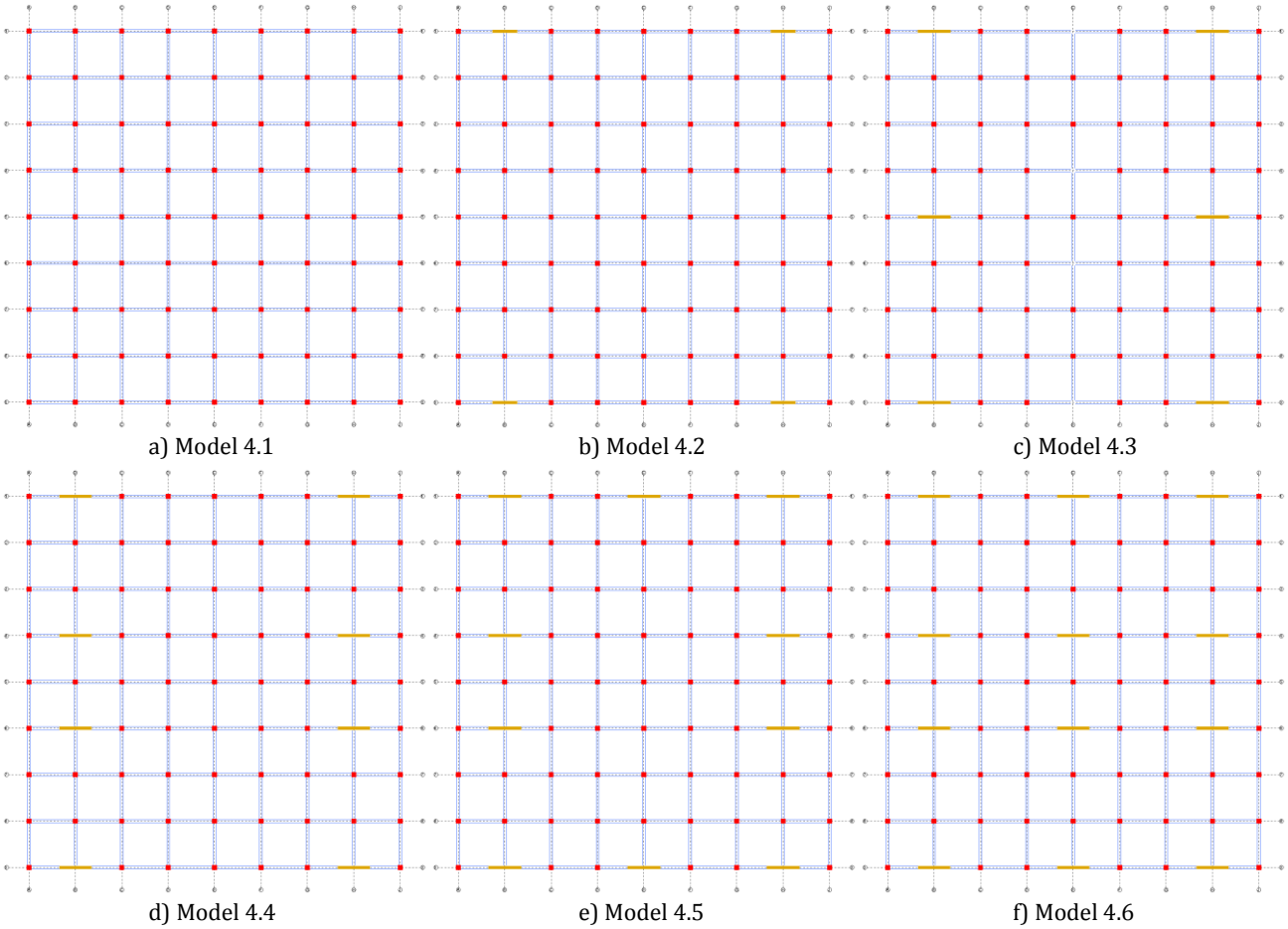

a) Model 4.1 b) Model 4.2 c) Model 4.3

d) Model 4.4 e) Model 4.5 f) Model 4.6

**Fig. 1.** (continued)

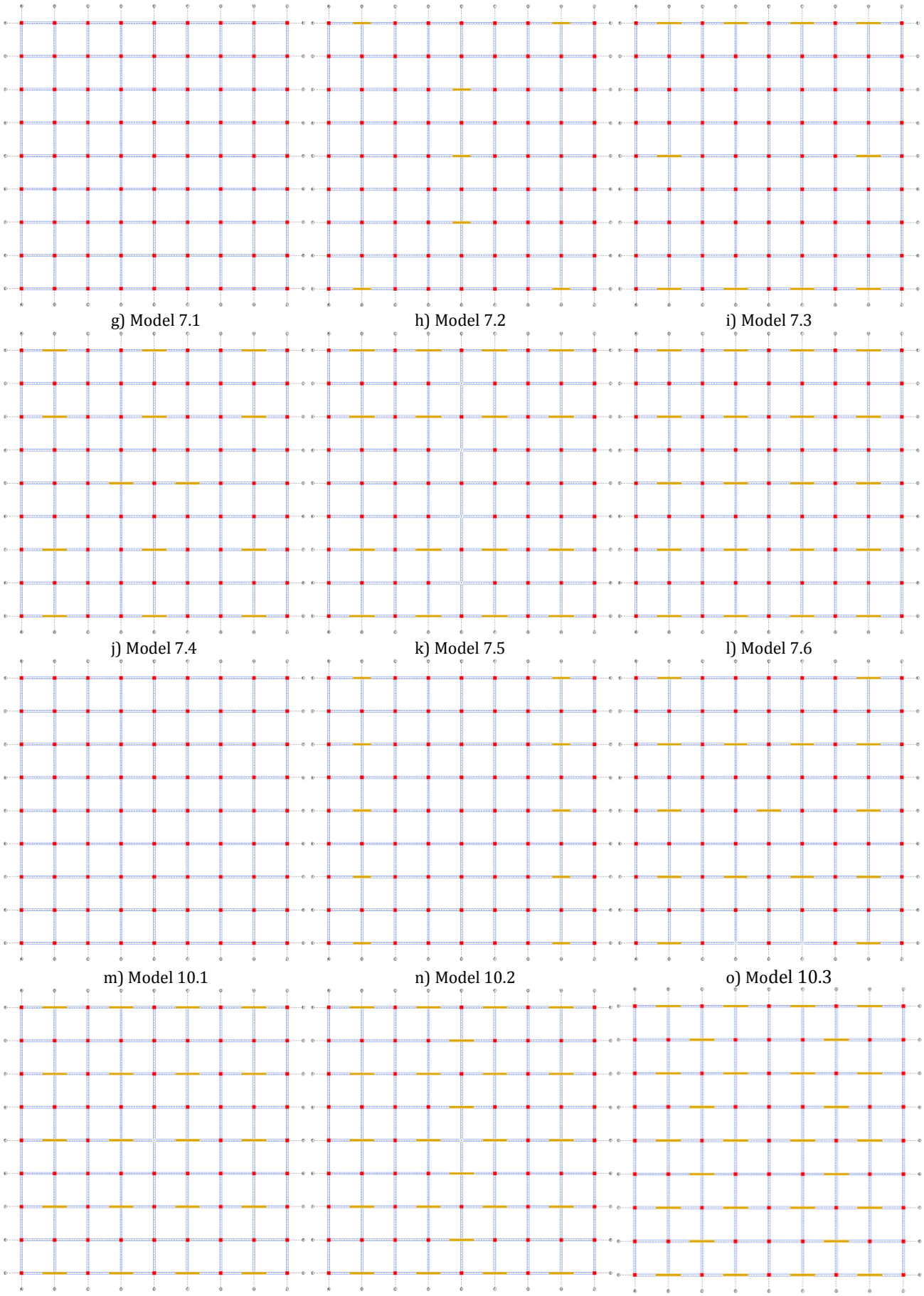


**Fig. 1.** Structural plans of models used in the study.

### 2.2. Load analysis

In the 18 types of analysis model prepared for this study, gravitational loads specified in TS498 are used. In order to determine the lateral loads, linear elastic analysis was performed by considering seismic loads calculated by Equivalent Seismic Load and Response Spectrum methods. The 15 cm thick slabs were not defined in the SAP2000 models and like the self weights of the slabs, the dead and live loads on the slabs were allocated to the beams as a line load which the slabs were connected. The columns and RC walls of the base story are fixed into the ground in the SAP2000 models. TS498 was used to determine the gravitational loads in order to design in accordance with the conditions specified by the regulations. In these analyzes, the gravitational loads applied to the models were calculated according to TS498 as follows:

- Slab self weight : 0.375 t/m$^2$
- Area dead load : 0.200 t/m$^2$
- Brick walls on beams : 0.500 t/m
- Area live load : 0.350 t/m$^2$
  - $\sum G_{slab}$ = 0.575 t/m$^2$
  - $\sum G_{brick}$ = 0.500 t/m
  - $\sum Q_{slab}$ = 0.350 t/m$^2$

Since the slabs are not modeled in the SAP2000 program, the loads transferred from these elements to the beams with the share of area are applied as triangular line load. The peak value of the triangular line loading condition is calculated as shown in Fig. 2.

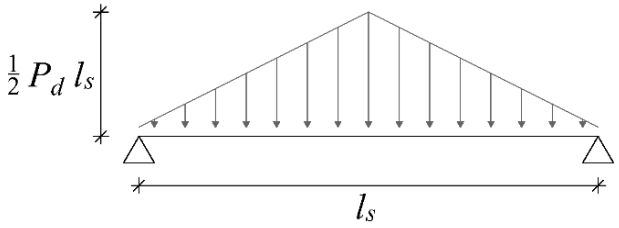


**Fig. 2.** Triangular line load distribution.

Triangular distributed load values calculated according to this diagram:

$G$ = [ 4 m x 0.575 t/m$^2$ ] / 2 = 1.15 t/m

$Q$ = [ 4 m x 0.35 t/m$^2$ ] / 2 = 0.7 t/m

However, these values are the load values to be loaded on the outer beams. Because loads from only one slab are transferred to the outer beams, load transfers from the two slabs are to the inner beams. Therefore, the values obtained were multiplied by two and the following loads were obtained and loaded on the inner beams:

$G$ = 1.15 t/m x 2 = 2.3 t/m

$Q$ = 0.7 t/m x 2 = 1.4 t/m

The load value of 0.5 t/m, which is determined as the brick wall load, is applied on the inner and outer beams as dead load. Rigid diaphragms have been defined for each story level as the solution will be made with the acceptance of rigid diaphragm.

According to this acceptance, story shear loads affect to center of the diaphragm.

### 2.3. Determination of earthquake parameters

18 analysis models have been created in 3 different building heights with the same floor areas. The story heights of the models are 3 m and the total building height is 12 meters for 4-storey models, 21 meters for 7-storey models and 30 meters for 10-storey models. The site class to be analyzed for these buildings is determined as ZC and the seismic level considered is DD-2. The building usage class is BKS-3 and the building importance coefficient is taken as $I$=1. For buildings with $S_{DS}$=1.327 and BKS-3, the seismic design class specified in TSC 2018 is $DTS$=1. $DTS$=1 and total building height values were taken into consideration and the building height class was found as $BYS$=6 for 4-storey models, $BYS$=5 for 7-storey models, and $BYS$=4 for 10-storey models.

The location determined for obtaining the parameters to be used in the calculation of seismic loads in accordance with TSC 2018 is the central Yakutiye district of Erzurum province. Fig. 3 shows the coordinates selected on Turkey Seismic Map arranged by MTA. (39.90601500°, 41.27772700°). (Disaster and Emergency Management Presidency, 2018).

Seismic parameters of this region with site class ZC and the earthquake level considered DD-2 are given:

| | |
|---|---|
| $PGA$ = 0.464 g | $PGV$ = 28.055 cm/sn |
| $S_S$ = 1.106 | $S_1$ = 0.288 |
| $S_{DS}$ = 1.327 | $S_{D1}$ = 0.432 |
| $T_A$ = 0.065 sn | $T_B$ = 0.325 sn |

Seismic parameters determined for linear analysis in accordance with TSC 2007; the 1st seismic zone and site class as Z3 (2007).

## 3. Analysis and Results

### 3.1. Equivalent seismic load method

Since the intended use of the designed buildings is determined as housing, the live load participation coefficients are taken as $n$=0.3 for both TSC 2007 and TSC 2018. The building masses are defined as $G$ + 0.3$Q$. The determined earthquake parameters are defined for 18 types of models and two different regulations on SAP2000 program.

The response modification coefficient of the models with 1st RC wall ratio (frame structural system) is $R$=8, the response modification coefficient of the RC wall ratio number 2 to 5 (wall-frame structural system) is $R$=7, for the buildings that have the RC wall ratio number 6 (RC wall structural system) response modification coefficient was selected as $R$=6. It should be noted that the Equivalent Seismic Load Method is not applicable for both regulations on 10-storey models used in this study. However, 10-storey models were also analyzed with this method in order to examine the results. Table 3 shows the percentage increase in the shear forces due to the shear ratio as compared to the reference models.

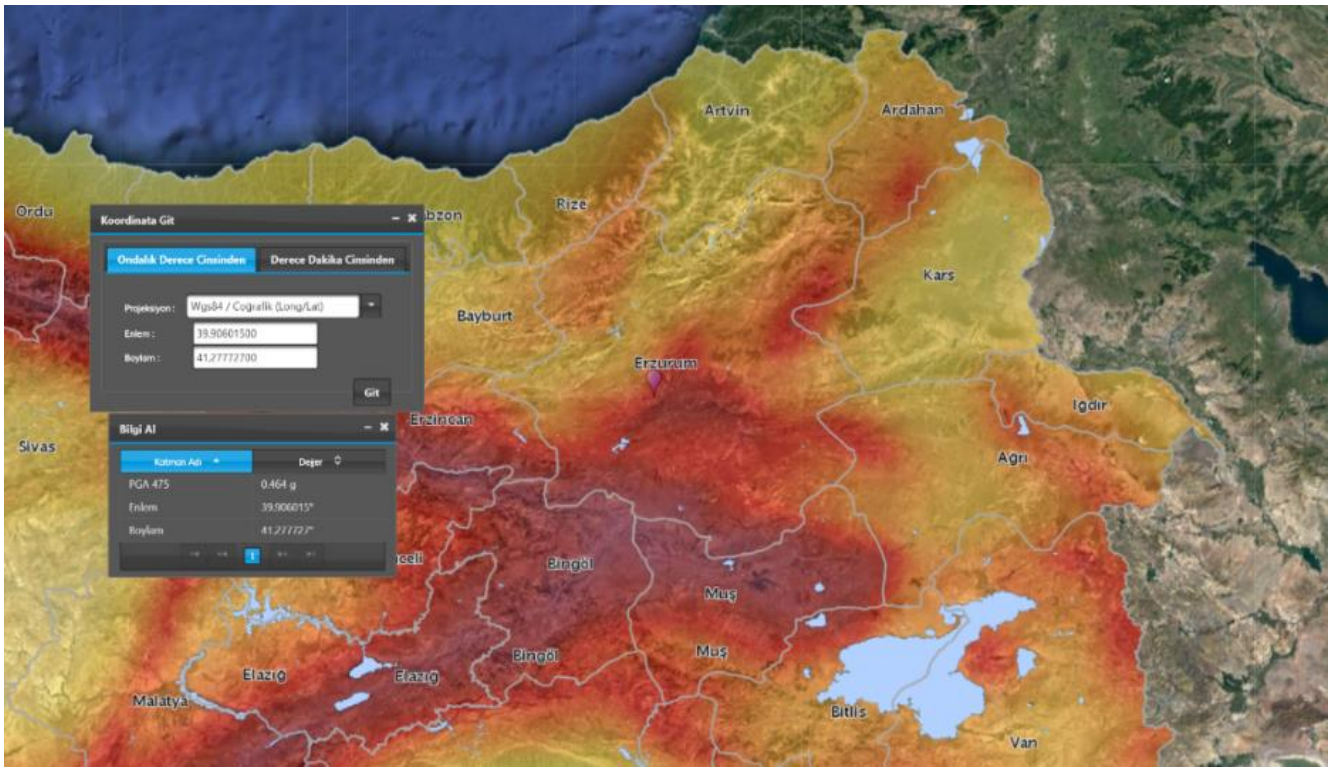


**Fig. 3.** Coordinates of the specified location.

**Table 3.** Percentage increase in the shear forces due to the shear wall ratio as compared to the reference models for equivalent seismic load method.

| RC Wall Ratio (‰) | 0 | 0.5 | 1 | 1.4 | 1.7 | 2 |
|---|---|---|---|---|---|---|
| 4 Story | 0 | 21.76 | 50.00 | 68.71 | 76.29 | 115.50 |
| 7 Story | 0 | 15.93 | 41.69 | 60.73 | 67.08 | 110.34 |
| 10 Story | 0 | 2.10 | 5.12 | 21.99 | 30.68 | 64.62 |

### *3.2. Response spectrum method*

This method does not have any restriction according to the geometric properties of the structures to be applied such as Equivalent Seismic Load Method. However, this method requires a more complex calculation. For this reason, analytical project design offices often use this method to determine seismic loads used in structural design. The response modification coefficients used for the models to be subjected to this analysis are the same as those used in the Equivalent Seismic Load Method. Spectrum curves were generated by using the functions given in the regulations and defined on the SAP2000 with the acceleration values corresponding to the period values used. For both regulations, only the base shear forces obtained from the results of the analyzed methods were compared. This method is defined in accordance with TSC 2018 and TSC 2007. Table 4 shows the percentage increase in the shear forces due to the shear ratio as compared to the reference models.

**Table 4.** Percentage increase in the shear forces due to the shear wall ratio as compared to the reference models for response spectrum method.

| RC Wall Ratio (‰) | 0 | 31.60 | 68.67 | 87.57 | 93.53 | 133.78 |
|---|---|---|---|---|---|---|
| 4 Story | 0 | 43.58 | 76.76 | 98.47 | 102.34 | 151.76 |
| 7 Story | 0 | 47.59 | 88.31 | 111.66 | 124.76 | 180.19 |
| 10 Story | 0 | 31.60 | 68.67 | 87.57 | 93.53 | 133.78 |

### *3.3. Analysis results*

18 types of building models are defined for 3 different building heights and 6 different RC wall ratios for each building height. These models were analyzed in accordance with the requirements of Equivalent Seismic Load Method and Response Spectrum Method specified in TSC 2018 and TSC 2007. These structures are designed regularly in the floor plan and the reinforced concrete RC wall elements are placed in the X direction in order to facilitate the comparison process and only the results in the X direction are considered for these two analysis methods.

The effects of the designs made according to both regulations on the mode periods were observed with the increase of the RC wall ratio. In Table 5, the comparison of the modal periods obtained with the designs made according to the two regulations as well as the base shear forces in the X direction obtained by the Equivalent Seismic Load Method and Response Spectrum Method applied according to TSC 2018 and TSC 2007 belonging to all models were made. Fig. 4 shows the graphs comparing the floor displacements prepared according to TSC 2018 and Fig. 5 according to TSC 2007.

When interpreting the values given in Table 5, it should be noted that 10-fold models among the models subjected to analysis are not suitable for the analysis according to the Equivalent Seismic Load method. Although this situation is known, the reason why the analyses have been applied on these models is to see what results will be encountered compared other suitable models. When interpreting Figs. 4 and 5, it should be noted that the seismic loads expected to be exposed to the structures are different in the analyses made using two different methods.

When the graphs given in Figs. 4 and 5 are examined, floor displacements of the reference models and the models with ‰ 0.5 RC wall ratio have received very large values for each building height. Against these values, the floor displacement values of the models with RC wall ratio ‰1 and more have decreased significantly, compared to the reference model. As a result of the analyzes made with two different calculation methods applied according to two different seismic codes, it is seen that the floor displacements do not decrease in accordance with the increase in the RC wall ratio when this ratio value exceeds ‰ 1. This result was obtained by examining detailed values that are in the tables given in the appendices (Table 6 to Table 17). In these tables, the obtained floor displacements of the buildings designed at three different building heights are given. According to the analysis results obtained for each building height subjected in this study, it can be suggested that the use of RC walls with a ratio of ‰ 1 is sufficient unless there is a demand for more base shear force.

## 4. Conclusions

In the analyzes carried out by the Equivalent Seismic Load Method, the base shear forces that will affect the structures have increased due to the increase of the RC wall ratio. In addition, the effect of response modification coefficients ($R$) is very important in this situation. However, it is not correct to say the same for story drifts. With the increase in the height of the building, the increased shear forces can be carried to a certain limit by the RC wall elements in the structural systems of the buildings. When the bending moments caused by the effect of lateral loads on the joints considered to be supported on the foundation of the structural system elements will increase as the building height increases. Increased story drifts caused by the shear forces that increased with building height, can be limited to a certain level by the RC wall elements placed in the structural systems of the buildings. These displacement values showed a linear increase up to the models with RC wall ratio ‰ 1, whereas the models with RC wall ratio greater than ‰ 1 showed a decreasing increase.

For all models and for both TSC 2007 and TSC 2018, the shear forces obtained by the Response Spectrum Method are lower than those obtained by the Equivalent Seismic Load Method. The reason for this is that the calculations made with the Equivalent Seismic Load Method are mainly based on the period values and story drifts of the 1st modes of the structures as well as the values obtained from the acceleration spectrum, conditional formulas and certain earthquake parameters according to the region where the structures will be built. On the other hand, Response Spectrum Method results are obtained by statistically combining the acceleration and period values obtained from the response spectrum for the region where the structures will be built.

It was found that the results of the base shear force obtained by the Equivalent Seismic Load Method increased with lower rates because the structures were dependent on the floor displacements and periods, but the total loads were larger. It can be concluded that the shear force results obtained by the Response Spectrum Method are lower than the Equivalent Seismic Load Method in total but Response Spectrum Method is more sensitive to the increasing stiffness of the structures. This sensitivity was observed with the percentage change of base shear force values which increased with the increase of RC wall ratio compared to the reference models.

The comments that can be made for the displacement values obtained as a result of the Response Spectrum Method may also be similar to the comments on the displacement values obtained as a result of the Equivalent Seismic Load Method. Because even if the different lateral loads affect the structure, the structural system will generate displacements depending on the amount of the loads applied.

**Table 5.** Comparison of analysis results according to TSC 2007 and TSC 2018.

| MODEL | RC Wall Ratio | EDY 2018 (ton) | EDY 2007 (ton) | MBY 2018 (ton) | MBY 2007 (ton) | MODAL 2018 | MODAL 2007 |
|---|---|---|---|---|---|---|---|
| Model 4.1 | 0 | 420.285 | 497.182 | 332.143 | 436.33 | 0.735 X<br>0.735 Y<br>0.680 T | 0.535 Y<br>0.535 X<br>0.496 T |
| Model 4.2 | 0.512 | 511.745 | 678.089 | 437.108 | 495.3544 | 0.734 Y<br>0.609 X<br>0.550 T | 0.535 Y<br>0.432 X<br>0.390 T |
| Model 4.3 | 1.007 | 630.487 | 728.965 | 560.216 | 583.8927 | 0.731 Y<br>0.499 X<br>0.488 T | 0.534 Y<br>0.353 X<br>0.347 T |
| Model 4.4 | 1.416 | 709.057 | 734.148 | 623.020 | 585.641 | 0.729 Y<br>0.468 T<br>0.447 X | 0.533 Y<br>0.332 T<br>0.316 X |
| Model 4.5 | 1.709 | 740.923 | 737.509 | 642.820 | 587.539 | 0.729 Y<br>0.434 T<br>0.429 X | 0.533 Y<br>0.307 T<br>0.303 X |
| Model 4.6 | 2.014 | 905.738 | 864.575 | 776.503 | 685.264 | 0.727 Y<br>0.437 T<br>0.412 X | 0.532 Y<br>0.309 T<br>0.290 X |
| Model 7.1 | 0 | 485.442 | 564.012 | 329.646 | 487.672 | 1.287 Y<br>1.287 X<br>1.189 T | 0.924 Y<br>0.924 X<br>0.856 T |
| Model 7.2 | 0.512 | 562.778 | 791.11 | 473.305 | 645.054 | 1.287 Y<br>1.035 X<br>0.996 T | 0.926 Y<br>0.728 X<br>0.703 T |
| Model 7.3 | 1.011 | 687.850 | 972.85 | 582.700 | 760.125 | 1.287 Y<br>0.816 X<br>0.766 T | 0.924 Y<br>0.574 X<br>0.536 T |
| Model 7.4 | 1.416 | 780.206 | 1071.408 | 654.261 | 822.472 | 1.282 Y<br>0.785 T<br>0.730 X | 0.921 Y<br>0.556 T<br>0.519 X |
| Model 7.5 | 1.702 | 811.069 | 1149.535 | 667.017 | 884.414 | 1.363 Y<br>0.722 T<br>0.707 X | 0.921 Y<br>0.488 T<br>0.479 X |
| Model 7.6 | 2.023 | 1021.058 | 1392.137 | 829.939 | 1070.8627 | 1.281 Y<br>0.722 T<br>0.661 X | 0.921 Y<br>0.505 T<br>0.462 X |
| Model 10.1 | 0 | 669.943 | 606.914 | 334.535 | 539.841 | 1.844 Y<br>1.844 T<br>1.701 B | 1.320 X<br>1.320 Y<br>1.218 T |
| Model 10.2 | 0.512 | 684.017 | 867.682 | 493.757 | 713.708 | 1.854 Y<br>1.450 X<br>1.449 T | 1.322 Y<br>1.0241 T<br>1.024 X |
| Model 10.3 | 1.007 | 704.289 | 1064.429 | 629.952 | 842.132 | 1.841 Y<br>1.280 T<br>1.156 X | 1.316 Y<br>0.906 T<br>0.817 X |
| Model 10.4 | 1.416 | 817.291 | 1211.478 | 708.092 | 939.018 | 1.843 Y<br>1.095 T<br>1.014 X | 1.315 Y<br>0.765 T<br>0.711 X |
| Model 10.5 | 1.699 | 875.468 | 1282.720 | 751.899 | 989.961 | 1.841 Y<br>1.061 T<br>0.959 X | 1.313 Y<br>0.742 T<br>0.672 X |
| Model 10.6 | 2.016 | 1102.871 | 1591.964 | 937.341 | 1220.435 | 1.839 Y<br>1.022 T<br>0.900 X | 1.311 Y<br>0.716 T<br>0.633 X |

X: represents the mode in X direction, Y: represents the mode in Y direction,
T: represents the mode in torsion.

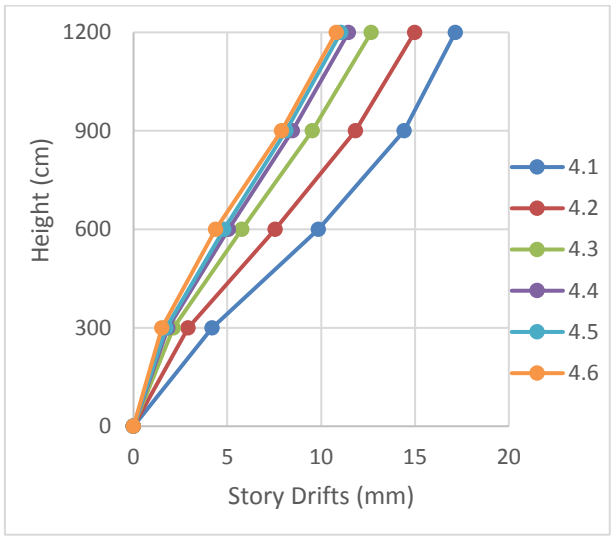


(a)

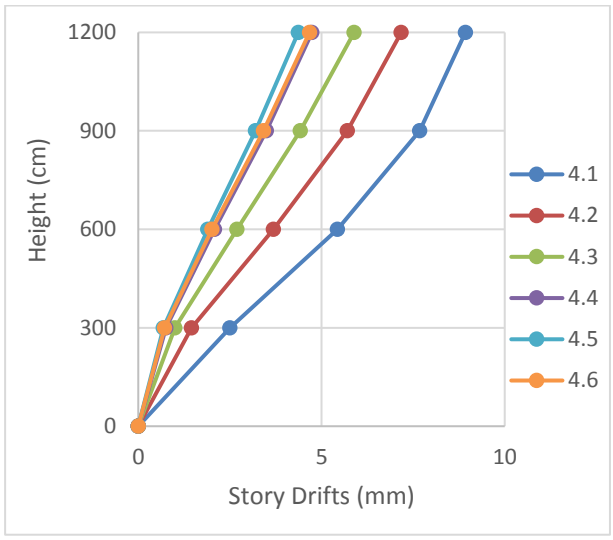


(b)

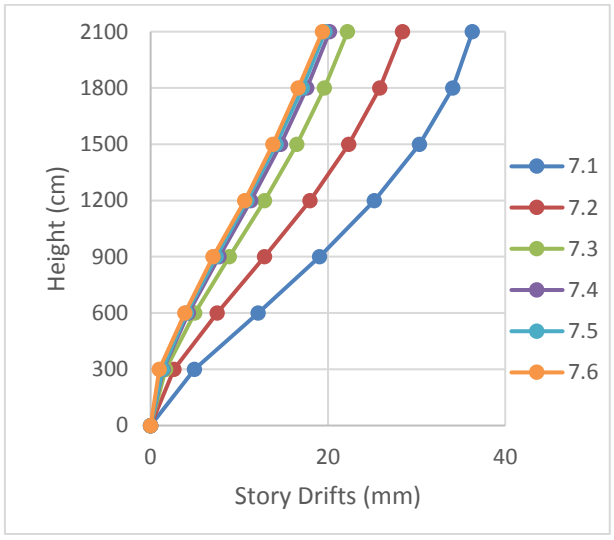


(c)

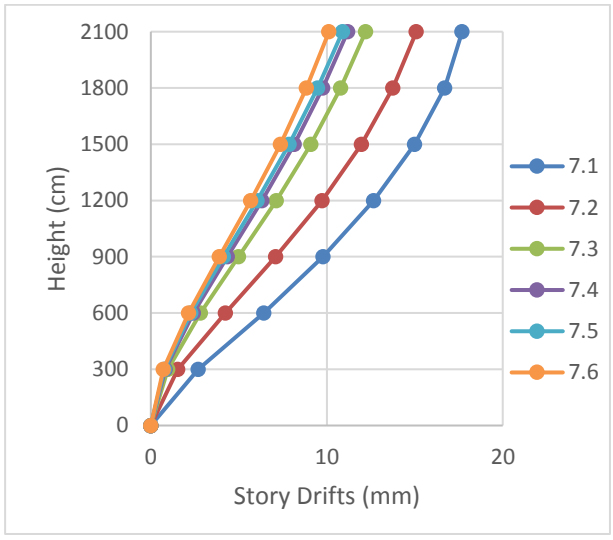


(d)

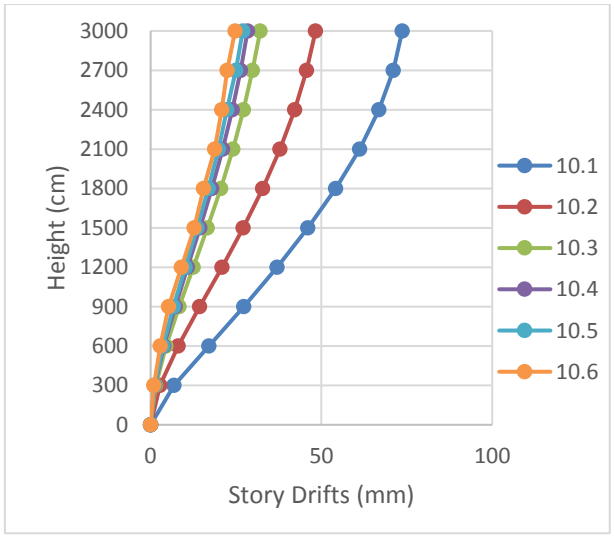


(e)

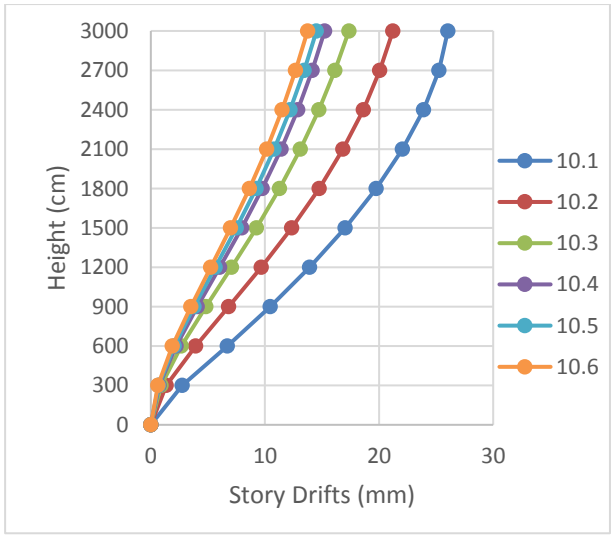


(f)

**Fig. 4.** Building height – story drifts curves for 4-storey, 7-storey and 10-storey models according to TSC 2018: a-c-e) Equivalent seismic load method; b-d-f) Response spectrum method.

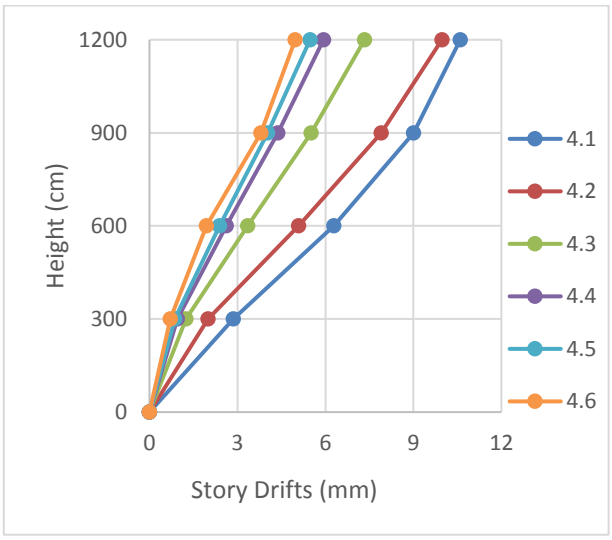


(a)

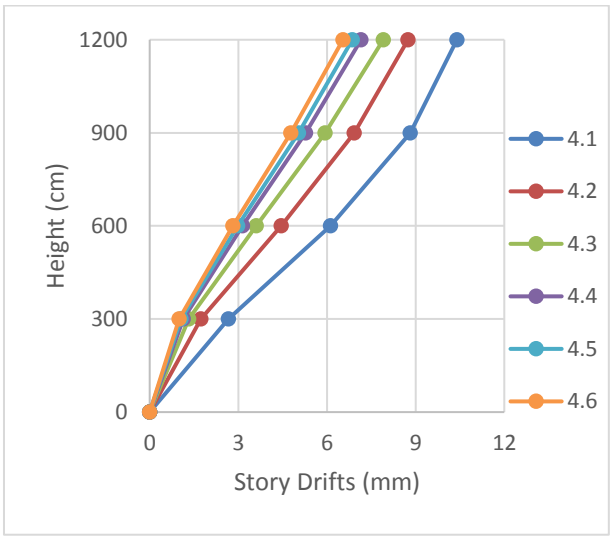


(b)

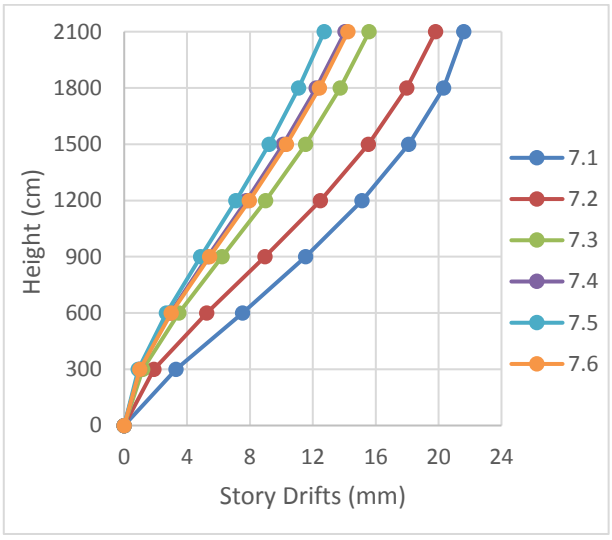


(c)

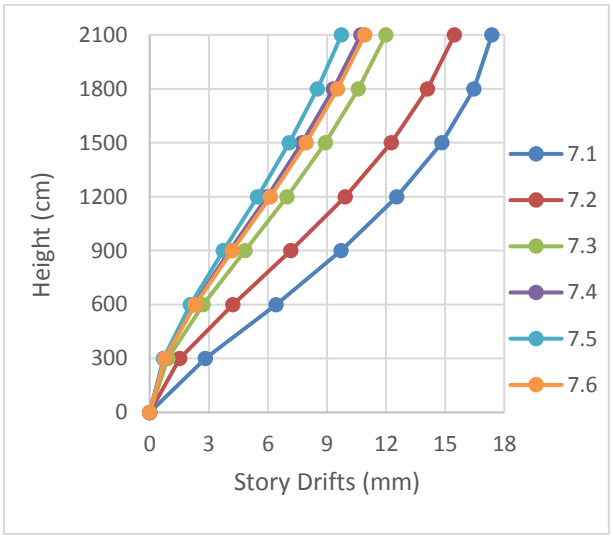


(d)

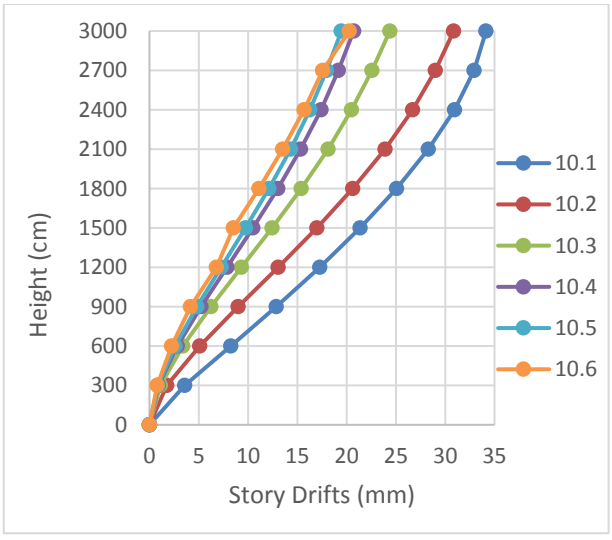


(e)

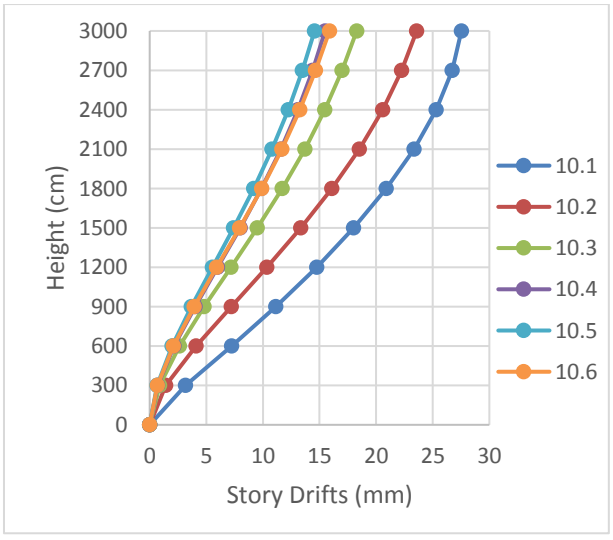


(f)

**Fig. 5.** Building height – story drifts curves for 4-storey, 7-storey and 10-storey models according to TSC 2007: a-c-e) Equivalent seismic load method; b-d-f) Response spectrum method.

The most ergonomic solution recommended to limit the displacements caused by lateral loads is that the optimum RC wall ratio to be determined is placed as symmetrical as possible and close to the outer edges of the building in the floor plan. In this way, the moment of inertia of the building to be obtained by multiplying the RC wall cross-sectional areas by the square of the distance between the element center of gravity and the structural systems center of gravity will increase and thus the bending stiffness of the structure will be increased and the structure will become more resistant to horizontal effects.

In the analyzes carried out by Equivalent Seismic Load Method and Response Spectrum Method specified in TSC 2018 and TSC 2007, the shear force values obtained in the calculations made according to TSC 2018 are lower than the results of the analyzes made according to TSC 2007 for both methods, and floor displacement values are higher in TSC 2018 models compared to TSC 2007 results. The main reason for this is the use of effective stiffness multipliers that must be defined on the structural system elements of the buildings to be modeled according to principles of Design by Strength.

## Appendix

**Table 6.** Displacement values of 4-storey models for equivalent seismic load method according to TSC 2007.

| Story Heights (cm) | Displacement Values (cm) | | | | | |
|---|---|---|---|---|---|---|
| | Model 4.1 | Model 4.2 | Model 4.3 | Model 4.4 | Model 4.5 | Model 4.6 |
| 300 | 2.8635 | 1.9992 | 1.2471 | 0.9557 | 0.8643 | 0.711 |
| 600 | 6.2889 | 5.0839 | 3.3566 | 2.6222 | 2.3959 | 1.9459 |
| 900 | 9.0072 | 7.9016 | 5.511 | 4.3829 | 4.0269 | 3.7997 |
| 1200 | 10.599 | 9.9733 | 7.3361 | 5.9341 | 5.4758 | 4.9701 |

**Table 7.** Displacement values of 4-storey models for response spectrum method according to TSC 2007.

| Story Heights (cm) | Displacement Values (cm) | | | | | |
|---|---|---|---|---|---|---|
| | Model 4.1 | Model 4.2 | Model 4.3 | Model 4.4 | Model 4.5 | Model 4.6 |
| 300 | 2.661 | 1.729 | 1.3268 | 1.1359 | 1.0651 | 0.9972 |
| 600 | 6.1213 | 4.4479 | 3.6042 | 3.1455 | 2.9828 | 2.8164 |
| 900 | 8.8222 | 6.9272 | 5.9386 | 5.2801 | 5.0377 | 4.7826 |
| 1200 | 10.398 | 8.7428 | 7.9073 | 7.1538 | 6.8594 | 6.5416 |

**Table 8.** Displacement values of 7-storey models for equivalent seismic load method according to TSC 2007.

| Story Heights (cm) | Displacement Values (cm) | | | | | |
|---|---|---|---|---|---|---|
| | Model 7.1 | Model 7.2 | Model 7.3 | Model 7.4 | Model 7.5 | Model 7.6 |
| 300 | 3.2951 | 1.8891 | 1.1926 | 0.9787 | 0.901 | 0.9963 |
| 600 | 7.5339 | 5.2603 | 3.4909 | 2.9283 | 2.6875 | 2.9941 |
| 900 | 11.557 | 8.9704 | 6.2273 | 5.3115 | 4.8666 | 5.4353 |
| 1200 | 15.138 | 12.491 | 8.9933 | 7.7838 | 7.1164 | 7.9561 |
| 1500 | 18.111 | 15.542 | 11.539 | 10.126 | 9.232 | 10.325 |
| 1800 | 20.318 | 17.978 | 13.738 | 12.221 | 11.105 | 12.421 |
| 2100 | 21.614 | 19.813 | 15.588 | 14.054 | 12.727 | 14.235 |

**Table 9.** Displacement values of 7-storey models for response spectrum method according to TSC 2007.

| Story Heights (cm) | Displacement Values (cm) | | | | | |
|---|---|---|---|---|---|---|
| | Model 7.1 | Model 7.2 | Model 7.3 | Model 7.4 | Model 7.5 | Model 7.6 |
| 300 | 2.8364 | 1.5263 | 0.9276 | 0.7489 | 0.6921 | 0.7661 |
| 600 | 6.4168 | 4.2311 | 2.7148 | 2.2428 | 2.067 | 2.306 |
| 900 | 9.7117 | 7.1725 | 4.8358 | 4.0676 | 3.7434 | 4.1878 |
| 1200 | 12.55 | 9.924 | 6.9682 | 5.9568 | 5.4702 | 6.127 |
| 1500 | 14.834 | 12.271 | 8.9184 | 7.742 | 7.0878 | 7.9428 |
| 1800 | 16.468 | 14.112 | 10.591 | 9.3328 | 8.5127 | 9.5406 |
| 2100 | 17.373 | 15.476 | 11.988 | 10.72 | 9.7401 | 10.916 |

**Table 10.** Displacement values of 10-storey models for equivalent seismic load method according to TSC 2007.

| Story Heights (cm) | Displacement Values (cm) | | | | | |
|---|---|---|---|---|---|---|
| | Model 10.1 | Model 10.2 | Model 10.3 | Model 10.4 | Model 10.5 | Model 10.6 |
| 300 | 3.5638 | 1.7505 | 1.112 | 0.9157 | 0.8362 | 0.7855 |
| 600 | 8.241 | 5.0848 | 3.3853 | 2.8123 | 2.5838 | 2.2499 |
| 900 | 12.865 | 9.0095 | 6.2443 | 5.2247 | 4.8208 | 4.1528 |
| 1200 | 17.276 | 13.058 | 9.3374 | 7.8534 | 7.2714 | 6.8018 |
| 1500 | 21.378 | 16.982 | 12.438 | 10.499 | 9.7499 | 8.4967 |
| 1800 | 25.08 | 20.628 | 15.396 | 13.026 | 12.128 | 11.098 |
| 2100 | 28.295 | 23.887 | 18.106 | 15.342 | 14.319 | 13.51 |
| 2400 | 30.935 | 26.684 | 20.507 | 17.394 | 16.272 | 15.677 |
| 2700 | 32.913 | 28.988 | 22.584 | 19.164 | 17.975 | 17.584 |
| 3000 | 34.143 | 30.859 | 24.387 | 20.715 | 19.468 | 20.272 |

**Table 11.** Displacement values of 10-storey models for response spectrum method according to TSC 2007.

| Story Heights (cm) | Displacement Values (cm) | | | | | |
|---|---|---|---|---|---|---|
| | Model 10.1 | Model 10.2 | Model 10.3 | Model 10.4 | Model 10.5 | Model 10.6 |
| 300 | 3.1568 | 1.42 | 0.866 | 0.7046 | 0.6412 | 0.675 |
| 600 | 7.2314 | 4.0988 | 2.6249 | 2.1608 | 1.9791 | 2.0948 |
| 900 | 11.144 | 7.206 | 4.8191 | 4.0051 | 3.6859 | 3.92 |
| 1200 | 14.759 | 10.355 | 7.1707 | 6.0018 | 5.5454 | 5.9232 |
| 1500 | 18.024 | 13.355 | 9.506 | 7.9954 | 7.413 | 7.9492 |
| 1800 | 20.899 | 16.101 | 11.712 | 9.8826 | 9.1909 | 9.8916 |
| 2100 | 23.341 | 18.524 | 13.717 | 11.597 | 10.815 | 11.68 |
| 2400 | 25.3 | 20.577 | 15.477 | 13.1 | 12.25 | 13.272 |
| 2700 | 26.711 | 22.245 | 16.985 | 14.387 | 13.487 | 14.66 |
| 3000 | 27.529 | 23.581 | 18.283 | 15.496 | 14.563 | 15.88 |

**Table 12.** Displacement values of 4-storey models for equivalent seismic load method according to TSC 2018.

| Story Heights (cm) | Displacement Values (cm) | | | | | |
|---|---|---|---|---|---|---|
| | Model 4.1 | Model 4.2 | Model 4.3 | Model 4.4 | Model 4.5 | Model 4.6 |
| 300 | 4.1957 | 2.9025 | 2.1243 | 1.8297 | 1.7296 | 1.5085 |
| 600 | 9.8451 | 7.5462 | 5.7799 | 5.059 | 4.8292 | 4.3691 |
| 900 | 14.422 | 11.838 | 9.5255 | 8.4761 | 8.1358 | 7.8898 |
| 1200 | 17.151 | 14.984 | 12.673 | 11.463 | 11.054 | 10.804 |

**Table 13.** Displacement values of 4-storey models for response spectrum method according to TSC 2018.

| Story Heights (cm) | Displacement Values (cm) | | | | | |
|---|---|---|---|---|---|---|
| | Model 4.1 | Model 4.2 | Model 4.3 | Model 4.4 | Model 4.5 | Model 4.6 |
| 300 | 2.5019 | 1.4522 | 0.9967 | 0.7583 | 0.6843 | 0.7189 |
| 600 | 5.4385 | 3.687 | 2.6902 | 2.0863 | 1.902 | 2.0162 |
| 900 | 7.6823 | 5.71 | 4.4229 | 3.4949 | 3.2044 | 3.4153 |
| 1200 | 8.9265 | 7.1775 | 5.8917 | 4.741 | 4.3672 | 4.6745 |

**Table 14.** Displacement values of 7-storey models for equivalent seismic load method according to TSC 2018.

| Story Heights (cm) | Displacement Values (cm) | | | | | |
|---|---|---|---|---|---|---|
| | Model 7.1 | Model 7.2 | Model 7.3 | Model 7.4 | Model 7.5 | Model 7.6 |
| 300 | 4.9549 | 2.6544 | 1.6861 | 1.4224 | 1.3405 | 0.9794 |
| 600 | 12.127 | 7.5051 | 4.9715 | 4.2684 | 4.0503 | 3.8724 |
| 900 | 19.066 | 12.879 | 8.8927 | 7.7382 | 7.3925 | 7.0425 |
| 1200 | 25.241 | 17.978 | 12.855 | 11.317 | 10.873 | 10.638 |
| 1500 | 30.346 | 22.373 | 16.493 | 14.676 | 14.171 | 13.806 |
| 1800 | 34.107 | 25.849 | 19.62 | 17.643 | 17.117 | 16.66 |
| 2100 | 36.311 | 28.407 | 22.221 | 20.192 | 19.691 | 19.38 |

**Table 15.** Displacement values of 7-storey models for response spectrum method according to TSC 2018.

| Story Heights (cm) | Displacement Values (cm) | | | | | |
|---|---|---|---|---|---|---|
| | Model 7.1 | Model 7.2 | Model 7.3 | Model 7.4 | Model 7.5 | Model 7.6 |
| 300 | 2.6939 | 1.5296 | 0.9728 | 0.8158 | 0.7619 | 0.7171 |
| 600 | 6.416 | 4.2329 | 2.8249 | 2.4202 | 2.284 | 2.1549 |
| 900 | 9.7979 | 7.1039 | 4.9864 | 4.3463 | 4.1382 | 3.8996 |
| 1200 | 12.667 | 9.736 | 7.1349 | 6.3114 | 6.0499 | 5.6878 |
| 1500 | 14.99 | 11.973 | 9.0951 | 8.1498 | 7.8559 | 7.3621 |
| 1800 | 16.699 | 13.755 | 10.788 | 9.7788 | 9.4746 | 8.8442 |
| 2100 | 17.694 | 15.092 | 12.21 | 11.188 | 10.897 | 10.127 |

**Table 16.** Displacement values of 10-storey models for equivalent seismic load method according to TSC 2018.

| Story Heights (cm) | Displacement Values (cm) | | | | | |
|---|---|---|---|---|---|---|
| | Model 10.1 | Model 10.2 | Model 10.3 | Model 10.4 | Model 10.5 | Model 10.6 |
| 300 | 6.884 | 2.7543 | 1.4781 | 1.2504 | 1.1565 | 0.9814 |
| 600 | 17.039 | 8.0889 | 4.5223 | 3.8613 | 3.5911 | 2.8698 |
| 900 | 27.264 | 14.387 | 8.3527 | 7.1907 | 6.7141 | 5.2618 |
| 1200 | 37.01 | 20.866 | 12.487 | 10.82 | 10.136 | 8.9981 |
| 1500 | 46.039 | 27.105 | 16.613 | 14.469 | 13.591 | 12.79 |
| 1800 | 54.154 | 32.845 | 20.521 | 17.943 | 16.896 | 15.435 |
| 2100 | 61.16 | 37.911 | 24.072 | 21.115 | 19.927 | 18.798 |
| 2400 | 66.867 | 42.182 | 27.181 | 23.908 | 22.314 | 20.797 |
| 2700 | 71.084 | 45.616 | 29.833 | 26.31 | 24.941 | 22.416 |
| 3000 | 73.65 | 48.297 | 32.09 | 28.38 | 26.962 | 24.711 |

**Table 17.** Displacement values of 10-storey models for response spectrum method according to TSC 2018.

| Story Heights (cm) | Displacement Values (cm) | | | | | |
|---|---|---|---|---|---|---|
| | Model 10.1 | Model 10.2 | Model 10.3 | Model 10.4 | Model 10.5 | Model 10.6 |
| 300 | 2.7667 | 1.3628 | 0.8883 | 0.7318 | 0.6728 | 0.6145 |
| 600 | 6.71 | 3.926 | 2.664 | 2.223 | 2.0588 | 1.8909 |
| 900 | 10.48 | 6.8313 | 4.8235 | 4.0747 | 3.7958 | 3.5052 |
| 1200 | 13.927 | 9.6916 | 7.073 | 6.0386 | 5.6537 | 5.247 |
| 1500 | 17.03 | 12.35 | 9.2525 | 7.9672 | 7.4919 | 6.9841 |
| 1800 | 19.755 | 14.745 | 11.281 | 9.7765 | 9.2271 | 8.6348 |
| 2100 | 22.063 | 16.845 | 13.116 | 11.42 | 10.811 | 10.15 |
| 2400 | 23.911 | 18.625 | 14.738 | 12.873 | 12.217 | 11.503 |
| 2700 | 25.249 | 20.073 | 16.144 | 14.135 | 13.444 | 12.689 |
| 3000 | 26.029 | 21.216 | 17.359 | 15.233 | 14.519 | 13.736 |

## REFERENCES


Arias H, Jaramillo JD (2019). Base shear determination using response-spectrum modal analysis of multi-degree-of-freedom systems with soil–structure interaction. *Bulletin of Earthquake Engineering*, 17(7), 1-14.

Arslan M, Olgun M, Köroğlu M, Erkan IH, Köken A, Tan O (2013). 19 May 2011 Kütahya–Simav earthquake and evaluation of existing sample RC buildings according to the TSC 2007 criteria. *Natural Hazards and Earth System Sciences*, 13(2), 505-522.

Dinçer F, Mert N (2014). Nonlinear static analysis of an existing reinforced concrete school building according to TSC 2007. *Sakarya University Journal of Science*, 18(1), 1-9.

Disaster and Emergency Management (2018). Turkish Seismic Hazard Maps Interactive Web App. AFAD, Ankara. https://tdth.afad.gov.tr/

Doğan TP (2019). An Investigation on Overstrength Factor İn Reinforced Concrete Buildings. *MSc thesis*, Konya Technical University, Konya, Turkey.

Erkan IH, Doğan TP, Arslan MH (2019). Investigation for overstrength factor in reinforced concrete shear walled buildings. *International Science and Academic Congress*, Konya, Turkey, 447-456.

Kıran F (2010). Examination of Linear and Nonlinear Analysis Methods for Performance Analysis of Buildings. *MSc thesis,* Çukurova University, Adana, Turkey.

Koçer M, Nakipoğlu A, Oztürk B, Al-Hagri MG, Arslan MH (2018). Comparison of main spectral acceleration values for seismic loads according to TSC 2018 and TSC 2007. *Selcuk-Technic Journal*, 17(2), 43-58.

Köse D (2008). Determination of the Performance Level of a Reinforced Concrete Structure by Incremental Equivalent Seismic Load Method. *MSc thesis,* İstanbul Technical University, İstanbul, Turkey.

Pakoğlu H (2009). Design of a Multi-Storey Building According to TSC 2007 and Theoretical Comparison of TSC 2007 and IBC. *MSc thesis,* İstanbul Technical University, İstanbul, Turkey.

TSC 2007 (2007). Turkish Seismic Code 2007. Ministry of Public Works and Settlement, Ankara, Turkey.

TSC 2018 (2018). Turkish Seismic Code 2018. Disaster and Emergency Management, Ankara, Turkey.

TS 498 (1997). Turkish Standards 498. Calculation values of loads to be taken in sizing of structural elements, Turkish Standardization Institute, Ankara, Turkey.

Uzun D (2014). The Effect of Different Slab Systems on Earthquake Behavior of a 33-storey Reinforced Concrete Building. *MSc thesis,* İstanbul Technical University, İstanbul Turkey.

Yılmaz C (2008). Performance Evaluation of an Existing Reinforced Concrete Structure by Static Pushover Analysis. *MSc thesis,* İstanbul Technical University, İstanbul, Turkey.

Challenge Journal of Structural Mechanics

Research Article

# Modification of the effective area method on two-way loaded shallow foundations

Mustafa Aytekin *

*Department of Civil Engineering, University of Bahrain, 32038 Isa Town, Kingdom of Bahrain*

**ABSTRACT**

In rectangular/square based and two-way loaded (two-way eccentric) shallow foundations, four zones in which the resultant load might act are defined in the effective area method. Three out of the four zones that are employed in the determination of the effective areas overlap around kern. Only one zone that has a triangular-shaped effective area (called as case 1 in the literature) out of the four zones has no overlap with the others. The resultant load will always be out of the kern for case 1, and also it might be out of the kern for the remaining three cases. Design of foundations is not acceptable in general if the resultant load acts out of the kern. In the present study, the four cases are reconsidered. The zones on which the resultant load can be acting for the four cases are modified because these zones are overlapped partly. The modification has been made to have clear borders between the zones. On top of that, zone 4 is divided into two. A new zone corresponding to the area of kern is defined as zone 5. The design will be accepted if the resultant load acts within zone 5 (the kern). Also, the graphs in use to determine the dimensions of the effective areas are eliminated since it is not precise. Formulas are derived to determine the dimensions of the effective areas instead of using the graphs. Two new criteria are discovered and proposed to check whether the resultant load acts outside, inside or on the borderline of zone 5 (the kern).

**ARTICLE INFO**

*Article history:*
Received 5 September 2019
Revised 13 November 2019
Accepted 24 November 2019

*Keywords:*
Shallow foundations
Two-way eccentricity
Effective area method
Bearing capacity

## 1. Introduction

The steps on the geotechnical design of two-way loaded (two-way eccentric) foundations are as follows:

**a.** Determine the eccentricities of $e_B$ and $e_L$ seen in Fig. 1 in both directions of $B$ and $L$, respectively.

**b.** Determine the dimensions of the kern as seen in Fig. 2, and check the location of the resultant load ($Q$) whether it acts inside, outside or on the borderline of the kern.

Use the criteria seen below to find out the location of the resultant load (Eq.(1)).

$$\left(\frac{6e_B}{B}+\frac{6e_L}{L}\right)\leq 1 \qquad (1)$$

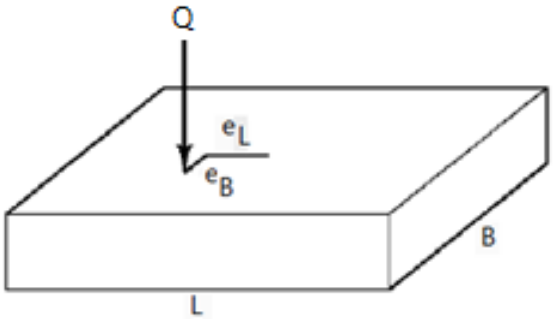


**Fig. 1.** Two-way loaded square/rectangular foundation.

If Eq. (1), which represents the last two terms the second parenthesis of Eq. (2) has the value equal to one, the minimum bearing pressure would be nil whereas if the

* *Corresponding author*. Tel.: +973-36936675 ; Fax: +973-17680843 ; E-mail address: maytekin@uob.edu.bh (M. Aytekin)
ISSN: 2149-8024 / DOI: https://doi.org/10.20528/cjsmec.2019.04.004

value is more than one, it would be a negative number, which means the minimum bearing is tension. In other words, if Eq. (1) is satisfied, the minimum bearing pressure is either compression or nil. Otherwise, the minimum bearing is a negative value that reflects a gap between the base of the foundation and underlying soil. Since no gap in the design is accepted under any foundation, there must be some solutions to avoid this situation like increasing dimensions of foundation or reducing the eccentricities physically.

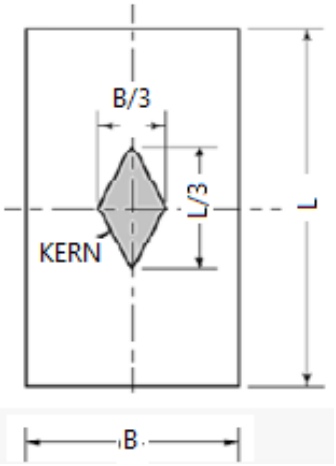


**Fig. 2.** Dimensions of the kern.

**c.** Use the sign (+ or -) in Eq. (2) to calculate the maximum and minimum bearing pressures at the base of foundation according to the position of the load (inside, or on the borderline of the kern).

$$q = \left(\frac{Q+W_f}{BL} - u_D\right)\left(1 \pm \frac{6e_B}{B} \pm \frac{6e_L}{L}\right) \quad (2)$$

where
$Q$ is load from superstructure,
$W_f$ is weight of foundation,
$B$ and $L$ are width and length of foundation,
$U_{Df}$ is pore water pressure at the base level of the foundation,
$e_B$ and $e_L$ are eccentricities on $B$ and $L$ directions, respectively.

In the design, the maximum bearing pressure must be less than or equal to the allowable bearing capacity of soil, and at the same time, the minimum bearing pressure must be compression or at least zero but not tension. Once, the maximum and minimum bearing pressures are estimated, allowable bearing capacity of the foundation must be determined too.
The bearing capacity of foundation can be estimated by several methods. Terzaghi's bearing capacity equation (Terzaghi, 1943) is widely used to estimate the ultimate bearing capacity of foundations even it has many limitations in practical applications. To minimize these limitations, many proposals have been made by researchers (Meyerhof, 1963; Prakash and Saran, 1971; Saran and Agarwal, 1993; Vesic, 1973; Sawwaf and Nazir, 2012; Krabbenhoft et al., 2012; Loukidis et al., 2008, Badakhshan and Noorzad, 2017, Sahu et al., 2019). One of these methods has been proposed by Meyerhof (1963) and his proposed method is known as "Meyerhof Bearing Capacity Equation, General Bearing Capacity Equation, or The Effective Area Method". Vesic (1973) has also proposed an equation almost identical with Meyerhof's equation. Meyerhof's general bearing capacity equation is seen below:

$$q_u = c'N_cF_{cs}F_{cd}F_{ci} + qN_qF_{qs}F_{qd}F_{qi} + 0.5\gamma B'N_\gamma F_{\gamma s}F_{\gamma d}F_{\gamma i} \quad (3)$$

where
$N_c$, $N_q$, $N_y$ are bearing capacity factors,
$F_{cs}$, $F_{qs}$, $F_{ys}$ are the shape factors,
$F_{cd}$, $F_{qd}$, $F_{yd}$ are the depth factors,
$F_{ci}$, $F_{qi}$, $F_{yi}$ are the inclination factors,
$c'$ is cohesion,
$q$ is effective stress at the base level of foundation,
$B'$ is the effective width of foundation,
γ is unit weight of soil.

Then, the ultimate bearing load can be estimated as follows.

$$Q_{\text{ult}} = q_uA' \quad (4)$$

A procedure to determine the effective area ($A'$) and effective width ($B'$) that would be used in the Meyerhof's general bearing capacity equation was proposed by (Highter and Anders, 1985) in addition to one proposed by Meyerhof (1963). It is the common practice to employ the proposed "effective area" determination on the design of two-way loaded foundations. In the determination of effective area, four cases are provided to design of square/rectangular based, and two-way loaded foundations by Highter and Anders in 1985. In the determination of the four cases, the criteria are the ranges of the ratios of $e_B/B$, and $e_L/L$. In general, nothing is mentioned for these four cases about the application points of the resultant loads whether it is in or out of the kern. However, anything may occur in terms of eccentricity. It means that the resultant force can be in, out or on the borderline of the kern except case 1 where eccentricity is always out of the kern.

## 2. Cases Defined in the Effective Area Method

When one has a closer look into the four cases mentioned in the event of effective area method, the resultant load is always out of the kern in case 1 seen in Fig. 3, mostly out of the kern in cases 2 (Fig. 4), and 3 (Fig. 5), some area out of the kern even in case 4 (Fig. 6). Thus, the cases should be modified to have a clear border between the cases. Only case 1 has the areas not overlap with the areas of the rest of the cases. There are overlaps of the areas in the cases of 2, 3, and 4 as seen in Figs. 4, 5, and 6. Zone 4 seen in Fig. 6 is the common zone in the cases of 2, 3, and 4. The shapes and borders of the effective areas are taken from Das (2007).

**CASE 1:** [$(e_L/L) > (1/6)$ and $(e_B/B) > (1/6)$]

As it is seen in Fig. 3, the resultant acts within the zones 1. It is obvious that the resultant load acts out of the kern so that minimum bearing pressure would be tension and a gap between the base of the foundation and the underlying soil would occur.

**CASE 2:** [$(e_L/L) < 0.5$ and $0 < (e_B/B) < (1/6)$]

As it is seen in Fig. 4, the resultant load acts within zone 2. Again, it is obvious that the resultant load is not always acting within or border line but mostly out of the kern so that minimum bearing pressure would be tension mostly and a gap between the base of foundation and the underlying soil would occur.

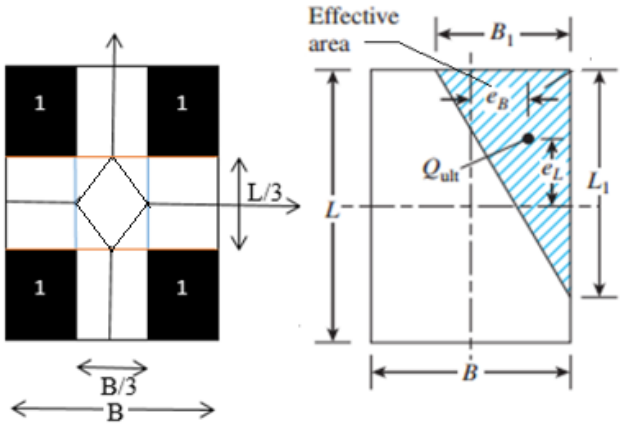


**Fig. 3.** Resultant load acts in zone 1 (Case 1).

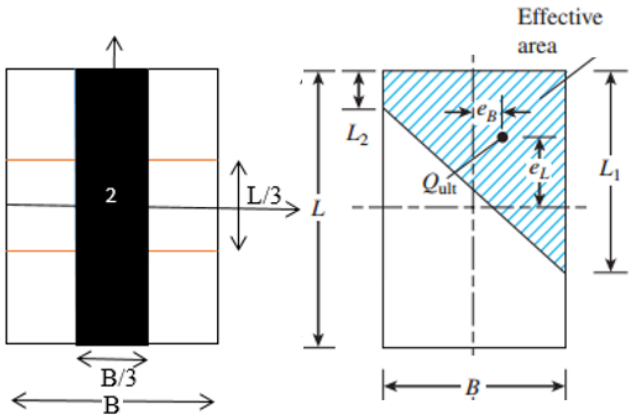


**Fig. 4.** Resultant load acts in zone 2 (Case 2).

**CASE 3:** [$(e_L/L) < (1/6)$ and $0 < (e_B/B) < 0.5$]

As it is seen in Fig. 5, the resultant load acts within zone 3. Again, the resultant load not always acts within or on the borderline but mostly out of the kern. Hence, minimum bearing pressure would be tension mostly and a gap between the base of the foundation and the underlying soil occurred.

**CASE 4:** [$(e_L/L) < (1/6)$ and $(e_B/B) < (1/6)$]

As it is seen in Fig. 6, the resultant load acts within zone 4. It acts within the kern or on its borderline, but also out of it. Thus, the minimum bearing pressure might be tension and a gap between the base of the foundation and the underlying soil might occur.

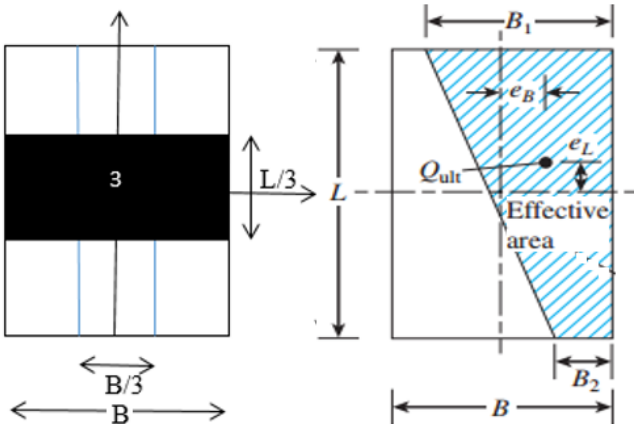


**Fig. 5.** Resultant load acts in zone 3 (Case 3).

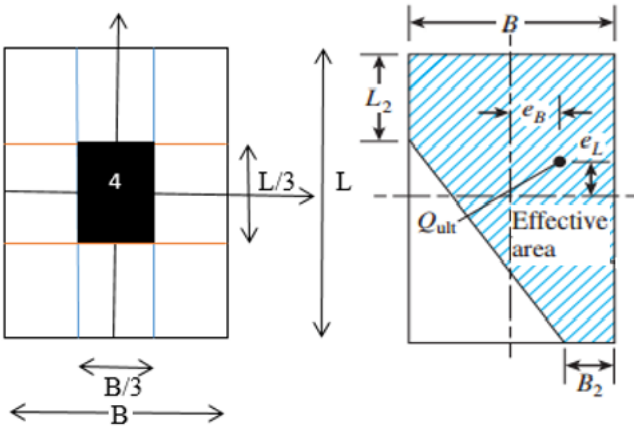


**Fig. 6.** Resultant load acts in zone 4 (Case 4).

## 3. Modified Cases

**CASE 1** has not changed so that the resultant load acts out of the kern all the time, while it is more often than out of the kern in cases of 2, 3, and 4. In the modified cases of 2, 3, and 4, the resultant load is out of the kern also. Thus, these cases may be studied in any research or other purposes except the design of foundations that would be applied in the field. The reason for that there would be tension between the base of foundation and underlying soil.

In this study, a new case is defined as "case 5" (Fig. 11) that is actually representing the kern so that case 5 can be used to design foundations that would be applied in the field because the resultant load acts in the kern so that the minimum bearing pressure would be a positive value or at least nil.

**Modified CASE 2**: Modified and redefined as seen below.

[$(1/6) < (e_L/L) < 0.5$ and $0 < (e_B/B) < (1/6)$]

When these ranges are applied to zone 2, it will become as seen in Fig. 7. The comparison between Figs. 4 and 7shows the difference.

The dimensions of the effective area seen in Fig. 4b can be calculated by the Eqs. (5 to 9) instead of using the graph generated in the original effective area method.

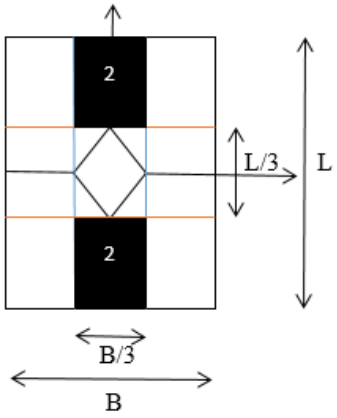


**Fig. 7.** Zone 2 after the modification.

$$A_o = \frac{B-6e_B}{B+6e_B} \tag{5}$$

$$L_1 = \left(\frac{1.5-3eL/L}{1+A_o+A_o^2}\right)(A_o+1)L \le L \tag{6}$$

$$L_2 = A_o L_1 \le L \tag{7}$$

The effective area;

$$A' = \frac{1}{2}(L_1 + L_2)B \tag{8}$$

and the effective width;

$$B' = \frac{A'}{L_1 or L_2 (\text{larger one})} \tag{9}$$

**Modified CASE 3:** Modified and redefined as seen below. [$(e_L/L) < (1/6)$ and $(1/6) < (e_B/B) < 0.5$]

When these ranges are applied to zone 3, it will become as seen in Fig.8. The difference can be seen by comparing Figs. 5 and 8.

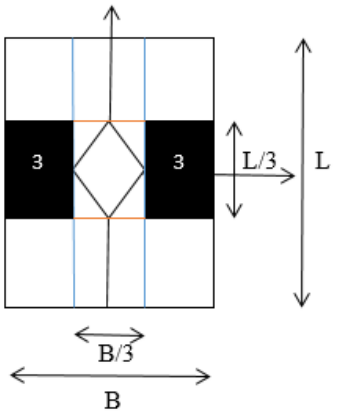


**Fig. 8.** Zone 3 after the modification.

The dimensions of the effective area seen in Fig. 4b can be calculated by the Eqs. (10 to 14) instead of using the graph generated in the original effective area method.

$$A_1 = \frac{L-6e_L}{L+6e_L} \tag{10}$$

$$B_1 = \left(\frac{1.5-3e_B/B}{1+A_1+A_1^2}\right)(A_1+1)B \le B \tag{11}$$

$$B_2 = A_1 B_1 \le B \tag{12}$$

The effective area;

$$A' = \frac{1}{2}(B_1 + B_2)L \tag{13}$$

and the effective width;

$$B' = \frac{A'}{L} \tag{14}$$

**Modified CASE 4:** The four dark triangular zones seen in Fig. 9 represent zone 4. The eccentricity of the resultant load would be within the following borders for this case.

$e > e_{\max}$, and $\frac{e_B}{B} \le \frac{1}{6}$ and $\frac{e_L}{L} \le \frac{1}{6}$

where $e$ and $e_{\max}$ are calculated from Eqs. (18 and 19), respectively. The effective area and effective width for this case would be calculated just like the procedure given in case 5.

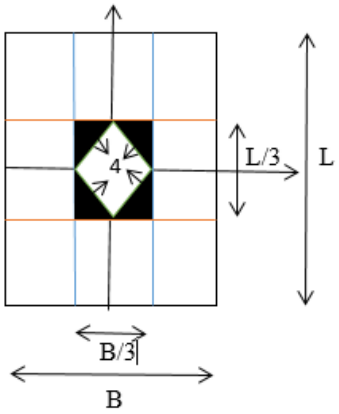


**Fig. 9.** Zone 4 after the modification.

**CASE 5 (New)**: A new case that envisages the zone of kern exclusively considered (see Fig. 10). Two criteria for this zone have been determined and given below. One of the criteria can be employed to determine whether the resultant load is within, on or out of the borderline of kern.

Criteria 1:

The kern is seen in Fig. 11a (zone 5), and one of the four parts of the kern is shown in Fig. 11b. To create a criteria that would be employed for the case 5 in the effective area method, the steps are as follows.

1. Find angles $\alpha$, $\beta$, and $\gamma$ in Fig. 11b as seen below.

$$\alpha = \tan^{-1}\left(\frac{B}{L}\right) \tag{15}$$

$$\beta = \tan^{-1}\left(\frac{e_B}{e_L}\right) \tag{16}$$

$$\gamma = 180 - \alpha - \beta \tag{17}$$

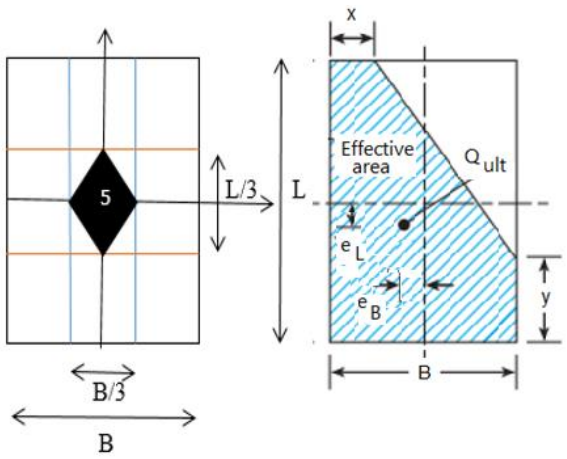


**Fig. 10.** Zone 5 newly defined.

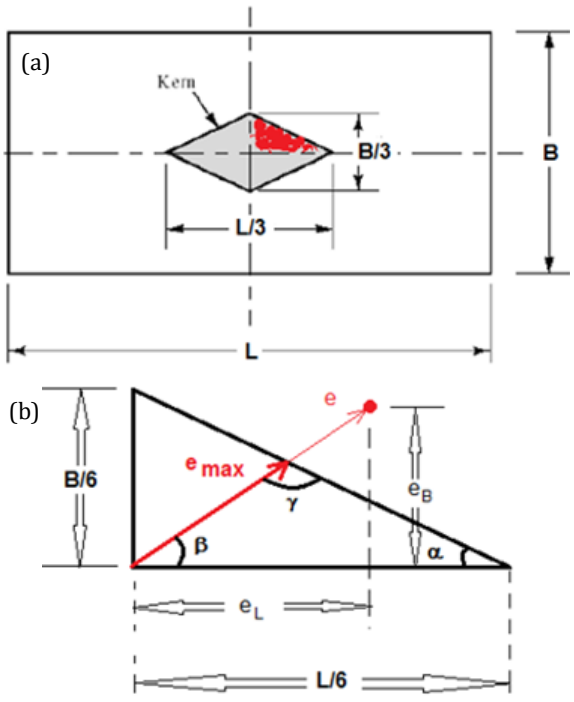


**Fig. 11.** The value of eccentricities on a foundation.

2. Find maximum value of eccentricity within the kern:

$$e_{\max} = \frac{\sin\alpha}{\sin\gamma} \cdot \frac{L}{6} \tag{18}$$

3. Find the existing eccentricity;

$$e = \sqrt{(e_L^2 + e_B^2)} \tag{19}$$

Application of resultant load is within the kern if $e < e_{max}$ .

Application of resultant load is on the borderline of the kern if $e = e_{max}$ .

Application of resultant load is outside of the kern if $e > e_{max}$ .

Finally, check up on criteria of the modified cases should $e$ be of less value than $e_{max}$ or equal to it, the technique met in case 5 applies.

Criteria 2:

To have the point of application of the resultant load within the kern, with the eccentricity on $B$-direction only, the maximum value of $e_B = B/6$ while the eccentricity on L-direction is equal to zero ($e_L = 0$); or vice versa with the eccentricity on $L$-direction only (see Fig. 12).

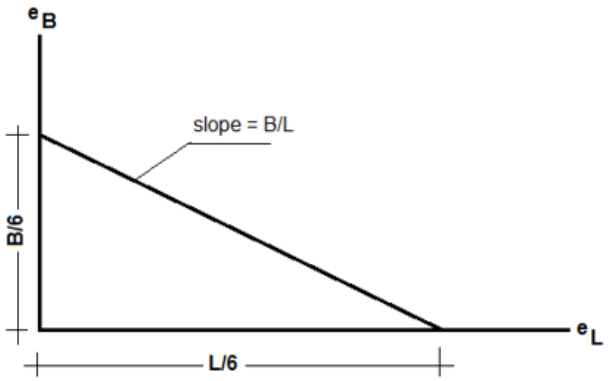


**Fig. 12.** One fourth of the kern.

Thus, the following relationships can be written:

$$\left[0 \le \frac{e_B}{B} \le \left(\frac{1}{6} - \frac{e_L}{L}\right)\right] \tag{20}$$

or

$$\left[0 \le \frac{e_L}{L} \le \left(\frac{1}{6} - \frac{e_B}{B}\right)\right] \tag{21}$$

If this is the case of eccentricities, the resultant load acts either in the kern or on its borderline. When this criterion is not satisfied, the resultant load is out of the kern, and the minimum value of the bearing pressure is a tension. In general, a foundation with tension under its base is not allowed to be constructed since there would be a gap between its base and underlying soil.

If the resultant load acts in zone 5, which is actually the kern, the shape of the effective area would be similar to one seen in Fig. 13b. Coordinates of the effective area can be located from 0 to 5 that must be numbered clockwise as seen in Fig 13a. The coordinates of the points (0 to 5) are numbered as follows:

$0(x_0,y_0)$, $1(x_1,y_1)$, $2(x_2,y_2)$, $3(x_3,y_3)$, $4(x_4,y_4)$, $5(x_5,y_5)$

Actually $x_0 = x_5$, and $y_0 = y_5$. From Fig. 13b:

$0(0,0)$, $1(0, L)$, $2(x, L)$, $3(B, y)$, $4(B,0)$, $5(0,0)$ can be written.

Coordinates ($C_x$, and $C_y$) of the centroid of effective area can be written as follows (see Fig. 13b):

$$C_x = \frac{B}{2} - e_B \tag{22}$$

$$C_y = \frac{L}{2} - e_L \tag{23}$$

Also, these coordinates can be written as follows:

$$A = \frac{1}{2}\sum_{i=0}^{n-1}(x_i y_{i+1} - x_{i+1} y_i) \tag{24}$$

$$C_x = \frac{1}{6A}\sum_{i=0}^{n-1}(x_i + x_{i+1})(x_i y_{i+1} - x_{i+1} y_i) \quad (25)$$

$$C_y = \frac{1}{6A}\sum_{i=0}^{n-1}(y_i + y_{i+1})(x_i y_{i+1} - x_{i+1} y_i) \quad (26)$$

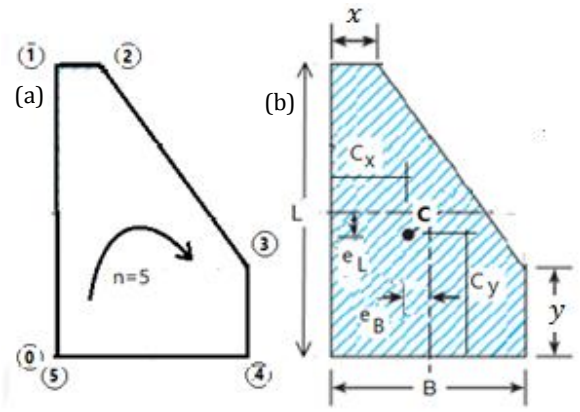


**Fig. 13.** Coordinates of effective area.

The right side of Eq. (25) is equal to the right side of Eq. (22), and Eq. (26) is equal to Eq. (23). Therefore, Eqs. (27) and (28) can be derived as follows:

$$-x^2 L + (x + B)(xy - BL) - 2B^2 y - 3\left(\frac{B}{2} - e_B\right)(-xL + xy - BL - By) = 0 \quad (27)$$

$$2xL^2 + (L + y)(xy - BL) - By^2 - 3\left(\frac{L}{2} - e_L\right)(-xL + xy - BL_{By}) = 0 \quad (28)$$

Eqs. (27) and (28) can be solved numerically for unknown $x$ and $y$ by a proper method. In this study, a MATLAB code has been developed to solve these equations and normalized values are given in Table 1. The effective area can be determined from:

$$A' = \frac{1}{2}(BL + xL + By - xy) \quad (29)$$

or

$$A' = \frac{1}{2}(B + x)(L - y) + By \quad (30)$$

or

$$A' = BL - \frac{1}{2}(B - x)(L - y) \quad (31)$$

and the effective width;

$$vB' = \frac{A'}{L} \quad (32)$$

Tables 1 and 2 can be used to determine effective areas for case 4 just like newly described case 5.

**Table 1.** $x/B$ values.

| $e_L/L$ | 0.027 | 0.053 | 0.080 | 0.107 | 0.133 | 0.160 |
|---|---|---|---|---|---|---|
| $e_B/B$ | | | $x/B$ | | | |
| 0.02 | 0.4614 | -- | -- | -- | -- | -- |
| 0.04 | 0.7380 | 0.3408 | 0.0625 | -- | -- | -- |
| 0.06 | 0.7323 | 0.5006 | 0.2389 | 0.0519 | -- | -- |
| 0.08 | 0.6976 | 0.5352 | 0.3303 | 0.1491 | 0.0124 | -- |
| 0.10 | 0.6539 | 0.5250 | 0.3628 | 0.2027 | 0.0688 | -- |
| 0.12 | 0.6090 | 0.4982 | 0.3633 | 0.2244 | 0.1000 | -- |
| 0.14 | 0.5636 | 0.4642 | 0.3475 | 0.2259 | 0.1125 | 0.0144 |
| 0.16 | 0.5184 | 0.4272 | 0.3232 | 0.2150 | 0.1120 | 0.0204 |

**Table 2.** $y/L$ values.

| $e_L/L$ | 0.027 | 0.053 | 0.080 | 0.107 | 0.133 | 0.160 |
|---|---|---|---|---|---|---|
| $e_B/B$ | | | $y/L$ | | | |
| 0.02 | 0.7819 | 0.7823 | 0.7256 | 0.6634 | 0.6006 | 0.5386 |
| 0.04 | 0.3254 | 0.6211 | 0.6249 | 0.583 | 0.5304 | 0.4747 |
| 0.06 | 0.0477 | 0.3894 | 0.4853 | 0.4812 | 0.4469 | 0.4021 |
| 0.08 | -- | 0.1901 | 0.3303 | 0.3655 | 0.354 | 0.3232 |
| 0.10 | -- | 0.0167 | 0.1902 | 0.2495 | 0.2584 | 0.2419 |
| 0.12 | -- | -- | 0.0756 | 0.1439 | 0.1667 | 0.1623 |
| 0.14 | -- | -- | -- | 0.0530 | 0.0833 | 0.0879 |
| 0.16 | -- | -- | -- | -- | 0.0100 | 0.0204 |

## 4. Conclusions

The following conclusions are drawn after the analytical and numerical work done in this study.

- Clear borders among the four zones are established without overlaps. That means borders of the zones given in the technical literature are modified.
- Zone 4 is divided into two. In other words, zone 4 has been modified and a new zone (zone 5) is defined.
- To check whether the resultant load acts in zone 5 (kern), two more criteria have been derived in addition to one in use.
- To calculate the effective areas for the defined five zones, formulas have been derived instead of employing the graphs in calculation of effective areas for all of the cases.
- Since the hand solution of formulas for zone 4, and 5 is impossible, a MATLAB code is generated and the equations are solved. However, any other numerical technique can be employed to solve the equations of (27) and (28).

## REFERENCES

Badakhshan E, Noorzad A (2017). A simplified method for prediction of ultimate bearing capacity of eccentrically loaded foundation on geogrid reinforced sand bed. *International Journal of Geosynthetics and Ground Engineering*, 3(2), 1-15.

Das MB (2007). Principles of Foundation Engineering. 6th edition, CENGAGE Learning, Hampshire, UK.

Highter WH, Anders JC (1985). Dimensioning footings subjected to eccentric loads journal of geotechnical engineering. *Journal of Geotechnical Engineering, ASCE*, 111(5), 659-665.

Krabbenhoft S, Damkilde L, Krabbenhoft H (2012). Lower-bound calculations of the bearing capacity of eccentrically loaded footings in cohesionless soil. *Canadian Geotechnical Journal*, 49(3), 298-310.

Loukidis D, Chakrabory T, Salgado R (2008). Bearing capacity of strip footings on purely frictional soil under eccentric and inclined loads. *Canadian Geotechnical Journal*, 45(6), 768-787.

Meyerhof GG (1953). The bearing capacity of foundations under eccentric and inclined loads. *Proceedings, 3rd International Conference on Soil Mechanics and Foundation Engineering*, Zurich, Vol. 1, 440-445.

Meyerhof GG (1963). Some recent research on the bearing capacity of foundations. *Canadian Geotechnical Journal*, 1(1), 16-26.

Prakash S, Saran S (1971). Bearing capacity of eccentrically loaded footings, *Journal of the Soil Mechanics and Foundation Division, ASCE*, 97(SM1), 95-117.

Sahu R, Patra CR, Sobhan K, Das BM (2019). Ultimate Bearing Capacity Prediction of Eccentrically Loaded Rectangular Foundation on Reinforced Sand by ANN. *In: Meguid M, Guler E, Giroud J (eds) Advances in Geosynthetics Engineering*. GeoMEast 2018. Sustainable Civil Infrastructures. Springer, Cham.

Terzaghi K (1943). Theoretical Soil Mechanics. Wiley, New York.

Vesic AS (1973). Analysis of ultimate loads of shallow foundations. *Journal of the Soil Mechanics and Foundation Division, ASCE*, 99(SM1), 45-73.